HHS Public Access

Author manuscript

J Struct Biol. Author manuscript; available in PMC 2019 November 01.

Published in final edited form as:

J Struct Biol. 2018 November ; 204(2): 151–164. doi:10.1016/j.jsb.2018.07.017.

Contributions of different modules of the plasminogen-binding *Streptococcus pyogenes* M-protein that mediate its functional dimerization

Cunjia Qiu[1,2], **Yue Yuan**[1], **Jaroslav Zajicek**[1,2], **Zhong Liang**[1,2], **Rashna D. Balsara**[1,2], **Teresa Brito-Robinson**[1], **Shaun W. Lee**[1,3], **Victoria A. Ploplis**[1,2], and **Francis J. Castellino**[1,2,*]

[1]W.M. Keck Center for Transgene Research, University of Notre Dame, Notre Dame, IN 46556

[2]Department of Chemistry and Biochemistry, University of Notre Dame, Notre Dame, IN 46556

[3]Department of Biological Sciences, University of Notre Dame, Notre Dame, IN 46556

Abstract

Group A *Streptococcus pyogenes* (GAS) is a causative agent of pharyngeal and dermal infections in humans. A major virulence determinant of GAS is its dimeric signature fibrillar M-protein (M-Prt), which is evolutionarily designed in modules, ranging from a hypervariable extracellular N-terminal region to a progressively more highly conserved C-terminus that is covalently anchored to the cell wall. Of the >250 GAS isolates classified, only the subset of skin-trophic Pattern D strains expresses a specific serotype of M-Prt, PAM, that directly binds to host human plasminogen (hPg) *via* its extracellular NH_2-terminal variable A-domain region. This interaction allows these GAS strains to accumulate components of the host fibrinolytic system on their surfaces to serve extracellular functions. While structure-function studies have been accomplished on M-Prts from Pattern A-C GAS isolates with different direct ligand binding properties from PAM, much less is known regarding the structure-function relationships of PAM-type M-Prts, particularly their dimerization determinants. To examine these questions, PAMs from seven GAS strains with sequence variations in the NH_2-terminal ligand binding domains, as well as truncated versions of PAM, were designed and studied. The results from bioinformatic and biophysical analyses show that the different domains of PAM are disparately engaged in dimerization. From these data, we propose an experimentally-based model for PAM secondary and quaternary structures that is highly dependent on the conserved helical C-terminal C-D-domains. In addition, while the N-

*Correspondening author: Francis J. Castellino, W.M. Keck Center of Transgene Research, 230 Raclin-Carmichael Hall, University of Notre Dame, Notre Dame, IN 46556, Voice: 574-532-4580, fcastell@nd.edu.

Conflict of interest

The authors declare that they have no conflicts of interests with this work.

Data deposition

Backbone chemical shift assignments and corresponding experimental restraints used in the structure calculations for $AGL55_{NS88.2}$, $KTI55_{SS1448}$, and $VEK75_{AP53}$ have been deposited in the BioMagResBank with the accession numbers, 30389, 30390, and 30391, respectively. The coordinates of calculated structure ensembles have been deposited in the Protein Data Bank with accession codes 6BZJ ($AGL55_{NS88.2}$), 6BJK ($KTI55_{SS1448}$), and 6BZL ($VEK75_{AP53}$).

terminal regions of PAMs are variable in sequence, the binding properties of hPg and its activated product, plasmin, to the A-domain, remain intact.

Graphical Abstract

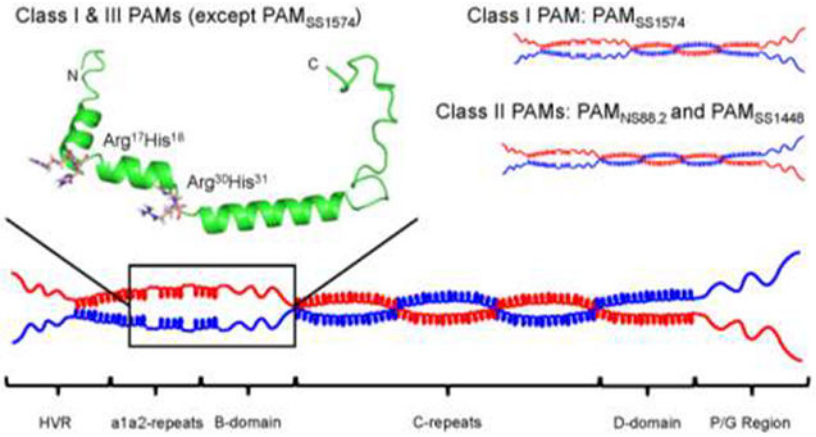

Keywords

Protein domains; protein chemistry; protein-protein interaction; plasminogen; bacteria; receptor structure-function; recombinant protein expression

1. Introduction

Group A *Streptococcus pyogenes* (GAS) is a spherical Gram-positive β-hemolytic pathogen that selectively infects humans, causing a range of infections, from currently antibiotic-sensitive pharyngitis and impetigo to serious invasive diseases, such as necrotizing fasciitis and streptococcal toxic shock, with a mortality >25%. In addition, immune sequela of these infections, such as acute rheumatic fever (ARF), are common causes of heart disease worldwide (Lee et al., 2009a). Thus, the morbidity and sometimes mortal GAS infections represent serious burdens to human health.

Numerous virulence factors are present in GAS, ranging from those present on the bacterial chromosomal to those expressed by incorporated bacteriophages (Bao et al., 2014). The GAS genome is very plastic with many integration sites, and horizontal transfer with recombination of genetic materials between GAS strains (Bao et al., 2014) and between GAS strains with other β-hemolytic streptococcal strains (McNeilly and McMillan, 2014) lead to new isolates with variable properties that result from selective pressures from the immune system of human hosts.

All known GAS isolates contain a signature high copy number M-Protein (M-Prt), encoded by the *emm* gene. This is the most widely recognized virulence determinant of GAS. Approximately 250 different antigenically distinct M-Prt-types of GAS isolates have been identified through sequencing ~90 nucleotides in the hypervariable region (HVR) of the *emm* gene (Beall et al., 1996; Bessen, 2016). M-Prts contain ~350–450 amino acids arranged in a modular fashion (Hollingshead et al., 1986). The N-terminus is HVR, which is

sequentially followed by variable A- and B- domains and highly conserved C-, D-, and Pro/Gly-modules (Fischetti, 1989; Fischetti, 1991). The C-terminus of mature M-Prts includes a sortase A (LPXTG)-sensitive membrane spanning site, which, when fully processed, is covalently linked to cell wall peptidoglycans. Conformationally, the mature M-Prt is a fibrillar protein consisting primarily of α-helices interrupted by loops, with its N-terminal regions (HVR-A-B-C-D) protruding through the cell wall into extracellular solutions. This provides GAS with a hair-like surface and allows the binding of many different types of host proteins to variably interact with strain-specific M-Prts.

The *emm gene* is located within a virulence-determining region of the bacterial chromosome, *viz.,* the multiple gene activator (Mga) regulon (Hondorp and McIver, 2007), which can contain up to five other sortase A-anchored proteins (Liang et al., 2013). This entire regulon is situated between the *mga* and laminin binding protein *(lmb*) genes in Pattern D strains. Thus, the environmentally-sensitive transcriptional factor, Mga, is an important regulator of M-Prt expression (McIver and Scott, 1997; McIver et al., 1995). The number and arrangement of the genes in the Mga regulon is used to type the pattern of this chromosomal region. Five patterns (A-E) have been identified with different gene arrangements in this regulon (Bessen et al., 1996). The characterization of this region of the chromosome is important for association of the subject GAS strain with the epidemiology of GAS infections, as well as their tissue selectivities and virulences.

In many pattern A-C strains, GAS utilizes M-Prts for adherence and colonization on oral and skin epithelial cells (Berge and Sjobring, 1993; Walker et al., 2014) to provide the inflammatory response accompanying infection. In addition to direct causation of the infection, GAS has evolved survival mechanisms in different host niches to assist the organism in evasion of the host innate immune response. For example, several Pattern A-C M-Prts interact with hemostasis system proteins, *e.g.,* fibrinogen (Ghosh, 2011; Glinton et al., 2017), to provide fibrin that encapsulates the bacteria to allow their colonization. This serves as an initial protective antiphagocytosis mechanism. Some other M-Prts of the Pattern A-C class react with complement binding proteins, *e.g.,* C4BP, and Factor H (FH), through the HVR- region, and inhibit C3b deposition on GAS cells (Berggård et al., 2001; Gustafsson et al., 2013).

Pattern D GAS strains are unique with regard to binding of host proteins and are the only GAS subtype that directly interacts with human plasma plasminogen (hPg), a key component of the fibrinolytic system, through their M-Prts (PAM). This specific and very tight interaction occurs *via* the variable A-domains of PAM (Ringdahl et al., 1998; Rios-Steiner et al., 2001; Wang et al., 2010b; Wistedt et al., 1995). The hPg-PAM interaction is central to the pathogenesis of this microorganism (Sanderson-Smith et al., 2006b). PAM-bound hPg is activated by a secreted subtype (2b) of streptokinase (SK2b), produced only by Pattern D strains (Zhang et al., 2012; Zhang et al., 2013). This process results in formation of a serine protease plasmin (hPm) (Lahteenmaki et al., 2001), that remains bound to GAS, thereby providing GAS with a surface-bound protease that is employed to solubilize host fibrin that encapsulates the GAS cells to permit ultimate dissemination. In addition, cell-bound hPm serves to degrade extracellular matrix (ECM) components and cellular tight junctions thereby facilitating the invasion of GAS into deep tissues of the host (Sumitomo et

al., 2016; Wong et al., 1992). Thus, the exclusive PAM-hPg interaction generally favors virulence of GAS (Sanderson-Smith et al., 2008; Sun et al., 2004).

Isolated M-Prts are generally believed to exist as non-ideal coiled-coil dimers in solution (Ghosh, 2011; Phillips et al., 1981), but limited experimental biophysical evidence lies at the basis of this conclusion. Nonetheless, the relative population of dimeric M-Prts on the cell surface is not known but would be expected to be limited by spacing constraints of the covalently bound monomers. While the functions of M-Prts bound to GAS cells have received much attention, M-Prts are also released from the cell surface during invasive infections, principally by a bacterial secreted cysteine protease, SpeB (Berge and Björck, 1995), and by neutrophil proteases (Herwald et al., 2004). The soluble forms of these M-Prts retain much their functional N-termini and thus possess important functions as soluble proteins. Thus, the structure-function relationships of M-Prts in solution are equally important to a fuller understanding of these virulence factors. In this regard, Pattern D M-Prts are not nearly as well studied as Pattern A-C M-Prts (Cedervall et al., 1997; Ghosh, 2018), but we know that PAM dimers are present in solution and possess functional properties (Agrahari et al., 2013; Agrahari et al., 2016; Bhattacharya et al., 2014). However, some Pattern D GAS strains possess PAMs with significant sequence differences in their hPg-binding sites of the A-domain (Sanderson-Smith et al., 2007). It is of central importance to understand whether natural variations in these PAMs result in conformational differences that could affect their structure-function properties, since it is also not expected that the highly variable number of amino acids in the N-terminal domains of M-Prts (Cedervall et al., 1997; Fischetti, 1989; Fischetti et al., 1988; Ghosh, 2011; McNamara et al., 2008; Nilson et al., 1995; Stewart et al., 2016) are compatible with a generalization that these regions all exist as α-helical parallel coiled-coils of similar stability, even in solution. Thus, the determinants for secondary and quaternary structures of PAM, as well as functional interactions of PAMs, were investigated herein, using PAMs from different GAS isolates with variable N-terminal sequences.

2. Materials and methods

2.1. Bacterial strains and cultures

The GAS strains investigated are listed by their isolate names (and *emm* serotypes): AP53 (*emm53*), NS88.2 (*emm98.1*), NS223 (emm91), NS455 (emm52), SS1448 (*emm86.2*), SS1572 (*emm223*), SS1574 (*emm224*). The AP53 strain was provided by G. Lindahl (Lund, Sweden), strains NS88.2, NS223, and NS455 were gifts from M. J. Walker (Queensland, Australia) (Sanderson-Smith et al., 2006a), and strains SS1448, SS1572, and SS1574 were obtained from the Centers for Disease Control and Prevention. These GAS isolates were cultured at 37° C, 5% CO_2 on sheep blood agar plates (Teknova, Hollister, CA) or in Todd-Hewitt broth (BD Bacto, Franklin Lakes, NJ) supplemented with 1% (w/v) yeast extract (BD Bacto) (THY).

2.1. DNA manipulations, cloning constructs, and protein purification

Genomic DNAs of the GAS isolates described above were extracted as previously reported (Ward and Leigh, 2002). To construct *pam* expression plasmids, the coding sequence of each

PAM, excluding the N-terminal signal peptide and C-terminal LPXTG membrane insertion region, was amplified *via* the polymerase chain reaction (PCR). PCR was conducted using Phusion high-fidelity DNA polymerase (New England Biolabs, Ipswich, MA). The forward primer was designed specifically for each PAM, which was necessitated by their 5'-variabilities, while the reverse primer was the same for each *pam* and contained a sequence that encoded a His_6-tag for subsequent protein purification (Table S1). The PCR products as well as the plasmid, pET-28a (EMD4Biosciences, Darmstadt, Germany), were digested with Nco I and EcoR I (New England BioLabs) at 37° C. The digested PAM inserts and the vector were purified using the Wizard SV Gel and PCR Clean-Up System (Promega, Madison, WI). The digested PCR products and plasmid pET-28a were next ligated at 14° C overnight using T4 DNA ligase (New England BioLabs). *Escherichia coli* DH5α (Invitrogen, Carlsbad, CA) cells were transformed with ligated mixtures employing the MicroPulser Electroporation System (Bio-Rad, Hercules, CA). The transformed cells were then cultured on Luria Bertani (LB) agar plates supplemented with 40 μg/mL kanamycin. The plasmid DNAs of the surviving colonies were extracted for PCR screening, and sequence analysis using the EZNA plasmid DNA Midi Kit (Omega, Norcross, GA). The same cloning strategy was applied to truncated PAM_{AP53}, *viz.,* PAM_{AP53_short} (residues 42–175), PAM_{AP53_medium} (residues 42–207), and PAM_{AP53_long} (residues 42–338) (Zhang et al., 2012).

2.2. Protein expression and purification

An engineered vector pET-15b (Novagen, Gibbstown, NJ) was employed to construct plasmids for expression of shortened peptides, including $AGL55_{NS88.2}$ (residues 95–149 of $PAM_{NS88.2}$), $KTI55_{SS1448}$ (residues 85–139 of PAM_{ss1448}), and $VEK75_{AP53}$ (residues 97–171 of PAM_{AP53}). Standard digestions and ligations were carried out as above. Colony screening was conducted on LB agar plates containing 100 μg/mL ampicillin. The final expression plasmid sequentially contains an ATG initiation codon, a His_6-tag, the GB1 subunit of the GABA receptor used for enhanced solubility, a 9-residue linker, a thrombin cleavage site (LVPR↓GS), the peptide coding sequence, and a translation stop codon. Consequently, all recombinant peptides contained residual Gly-Ser at their N-termini. Tyr present in the sequences was used for concentration determinations by A_{280nm} measurements (Bhattacharya et al., 2014).

E. coli BL21/DE3 cells (New England BioLabs) were transformed with the expression plasmids. Protein expression and purification procedures for r-PAMs, unlabeled shortened peptides, and $^{13}C/^{15}N$-labeled peptides have been described previously (Yuan et al., 2017).

2.3. Protein identification and concentration determinations

The integrity of all proteins and peptides was confirmed by MALDI-TOF mass spectrometry on an Autoflex III spectrometer (Bruker Daltonics) (Tables 1, 2). To obtain accurate extinction coefficients at 280 nm of all full-length PAMs, as well as PAM_{AP53_long}, the A_{280nm} refractive index increments at 670 nm were measured on an Optima XL-1 analytical ultracentrifuge (Beckman Coulter, Brea, CA) using a synthetic boundary centerpiece (Babul and Stellwagen, 1969). The cell was loaded in one chamber with 400 μL sodium phosphate, pH 7.4, and 190 μL and the protein sample was placed in the connecting chamber. The

rotational speed at 20° C was increased to 3,000 rpm to allow a sharp boundary to be formed between solvent and protein and the refractive increment measured at 670 nm. All measurements were completed in ~10 min in order that diffusion of protein at the boundary was limited. The number of interference fringes at the boundary is proportional to the protein concentration (4.1 fringes = 1 mg/mL) (Babul and Stellwagen, 1969). The protein concentration was accordingly determined from fringe displacement data and this, along with the A_{280nm} of the protein solution, provided accurate extinction coefficients (Table S2). This method has not been verified with shorter peptides. Thus, these extinction coefficients were calculated with ExPASY based upon Trp or Tyr residues in the sequences.

2.4. Circular dichroism (CD)

Far-UV CD spectra were collected for r-PAMs for secondary structure analyses. Measurements were made on an Aviv model 202 SF Spectrometer (Aviv, Lakewood, NJ) in 10 mM sodium phosphate/50 mM NaCl, pH 7.4. CD spectral data were continually recorded from 195 to 250 nm in the wavelength scan mode. Ellipticities were also monitored at 222 nm in the temperature scan mode, and collected from 4° C to 90° C. The spectra represented the average of three scans in both applications. An average buffer reference scan was subtracted from that of each sample. The mean residue ellipticities ($[\theta]$) of the protein/peptides were calculated using: $[\theta] = (\theta \times MRW)/(1 \times c)$, where θ is the original signal in mdeg, MRW is the mean residue weight in g/mol, l is the path length in mm, and c is the protein concentration in mg/mL (Greenfield, 2006). The α-helical content was estimated from $[\theta]_{222\ nm} = -30{,}300 f_H - 2{,}340$, in which f_H refers to the fraction of helices in the protein (Chen et al., 1972). The data were plotted using GraphPad Prism 7.

2.5. Analytical ultracentrifugation (AUC)

Sedimentation equilibrium analytical ultracentrifugation was performed at 25° C using an Optima XL-1 analytical ultracentrifuge (Beckman Coulter). The proteins/peptides were dissolved in 10 mM sodium phosphate/50 mM NaCl, pH 7.4, and diluted to A_{280nm} ~ 0.1 prior to loading. Three channels of a six-channel centerpiece were loaded with the buffer as a reference solution and protein samples were added to the adjacent channels. Three cell housings, containing one centerpiece each, were assembled and placed into a Beckman An-60 Ti rotor, together with the counterbalance (Bhattacharya et al., 2014). Samples were rotated individually at the speeds of 18,000 and 20,000 rpm for all full-length PAMs; 28,000, 32,000 and 36,000 rpm for PAM_{AP53_short}; 24,000, 28,000 and 32,000 rpm for PAM_{AP53_medium}; 18,000, 21,000, and 24,000 rpm for PAM_{AP53_long}. Scans were recorded hourly at 280 nm until three scans overlapped, at which point equilibrium was attained. The partial specific volume of each protein or peptide was calculated from the amino acid compositions using Sednterp (Table S2). The density of the buffer was 1 g/mL. Apparent weight average molecular weights for the whole sample were calculated from non-linear fitting of the data with Optima XL-A/XL-I data analysis software (Beckman Coulter), using concentration data from the meniscus (c_m) to the cell bottom (c_b) (Schuck et al., 2014). AUC sedimentation equilibrium assays were conducted in triplicate for each peptide or protein.

2.6. Helical wheel modeling

Helical wheel diagrams (Schiffer and Edmundson, 1967) for each domain in different PAMs were constructed in the parallel mode through the online server DrawCoil 1.0.

2.7. Nuclear magnetic resonance (NMR)

NMR spectra were recorded at 25° C on a Bruker AVANCE 800 spectrometer, equipped with a 5 mm triple resonance (TCI, ^{1}H, ^{13}C, ^{15}N) cryoprobe, for both resonance assignments and NOE identifications. All $^{13}C/^{15}N$-labeled peptides, *viz.* $AGL55_{NS88.2}$, $KTI55_{ss1448}$, and $VEK75_{Ap53}$, were dissolved in 20 mM BisTris-d19/2 mM 4,4-dimethyl-4-silapentane-1-sulfonic acid (DSS)/0.1% NaN_3, and 5% $^{2}H_2O$/95% H_2O, pH 6.7. The NMR data were processed with Bruker TopSpin 3.5 and analyzed with Sparky (Lee et al., 2009b). ^{1}H chemical shifts were referenced to internal DSS, whereby C and N chemical shifts were indirectly referenced to DSS (Markley et al., 1998). For resonance assignments of the peptide backbone and side chains, the following pulse sequences were used: ^{15}N-HSQC (Kay et al., 1992; Mori et al., 1995), HNCO/HN(CA)CO (Clubb et al., 1992; Kay et al., 2011), HNCA (Löhr and Rüterjans, 2002), HNCACB/CBCA(CO)NH (Wittekind and Mueller, 1993), (H)CC(CO)NH, and H(CC)(CO)NH (Löhr and Rüterjans, 2002). For intramolecular NOE distance restraints, both ^{15}N-NOESY-HSQC (Talluri and Wagner, 1996) and ^{13}C-NOESY-HSQC (Ikura et al., 1990) spectra were obtained.

2.8. NMR solution structures

The TALOS-N program was applied to predict the secondary structures of AGL55, KTI55, and VEK75 in their apo-forms based on assigned backbone chemical shifts (Shen and Bax, 2013). The CS-Rosetta program (Shen et al., 2009; Shen et al., 2008) was applied to generate the starting template for each peptide based on the chemical shifts. Structural calculations were then carried out with combined dihedral angle restraints (ϕ and ψ) from TALOS-N and the NOE restraints observed from 2D-NOESY and 3D-NOESY-HSQC experiments. Approximately 200 structures were generated through a simulated annealing protocol in the program Xplor-NIH 2.37 (Schwieters et al., 2006; Schwieters et al., 2018; Schwieters et al., 2003). Ten conformers with the lowest restraint energy values, and without distance and angle violations, were further refined with implicit water. The validity of the structures was analyzed PSVS version 1.5 with also integrates PROCHECK version 3.5.4 (Laskowski et al., 1993) in a single interface (Bhattacharya et al., 2007). Visualization of the structures was performed using PyMOL.

2.9. Surface plasmon resonance (SPR)

The binding kinetics of r-PAMs to hPg were measured *via* refractive index changes upon analyte/ligand binding in real-time using a BIAcore X100 Biosensor system (GE Healthcare). All binding experiments were conducted at 25° C. The running buffer was HBS-EP (10 mM Hepes, 0.15 M NaCl, 3 mM EDTA, 0.005% polysorbate 20, pH 7.4) flowed at 30 μL/min. hPg (30 μg/mL) in 10 mM sodium acetate, pH 4.5, was adsorbed onto flow cell-2 of a CM5 sensor chip (GE Healthcare), to a level of ~1,000 response units (RUs), using an amine coupling kit (GE Healthcare) (Bhattacharya et al., 2014; Chandrahas et al.,

2015; Glinton et al., 2017). Non-bound sites on the gold surface of sensor chip were subsequently blocked by injection of 1 M ethanolamine, pH 8.5.

In the binding experiments, various concentrations of analytes in HBS-EP buffer were injected for a 120 sec association time and a 360 sec dissociation time with hPg-coupled CM5 (Yuan et al., 2017). The gold surface was regenerated between cycles using 10 mM glycine, pH 2. The responses in flow cell-2 were subtracted from the background response of the analyte in the reference cell (flow cell-1) which does not contain immobilized ligand. The sensorgrams were analyzed using BIA evaluation software 2.0.1 (GE Healthcare). Equilibrium dissociation constants (K_D) were calculated from the ratio of the dissociation (k_{off}) and association rates (k_{on}). Nonlinear fitting of the association and dissociation curves with a 1:1 binding model was employed. Binding curves were presented in GraphPad Prism 7.

2.10. Flow cytometric analysis (FCA)

GAS cells were grown in THY media to an O.D.600nm of ~0.6 at 37° C, after which they were washed with phosphate-buffered-saline (PBS, pH 7.4) and then resuspended in PBS plus 1% ovalbumin for blocking. The cells were then incubated with hPg (ERL, South Bend, IN), after which the primary antibody, mouse-anti-hPg (ERL), was incubated with the cell suspensions. For detection of bound hPg, a secondary antibody, AlexaFluor 488-donkey-anti-mouse IgG (Invitrogen), was incubated with the cells. FCA was conducted using a FACSAria III (BD Biosciences) cytometer with the 488 nm laser at a flow rate of 10 μL/min, with 10,000 events recorded for analysis. Data were collected by gating on fluorescence (FITC-A) and on side-scatter.

The histograms obtained were then analyzed using FCS Express Version 4 software (De Novo Software, Los Angeles, CA). The median fluorescence intensity for each histogram was used to calculate the events accepted by the gating formula that fall within the specified marker. The percentage of anti-PAM or hPg-binding for each strain was normalized to strain, AP53, which was set at 100%. FCA of each GAS strain was conducted in triplicate, and all data were plotted using GraphPad Prism 7.

3. Results

3.1. Homology increases from N-termini to C-termini among different recombinant (r) PAMs

We selected seven recombinant (r)-PAMs from Pattern D GAS isolates to examine how the sequence variability affects the conformations, propensity to dimerize in solution, and the ligand binding properties of this class of M-Prt (Fig. 1A). PAM from the GAS AP53 (PAM_{AP53}) isolate was chosen as the prototype PAM for this work since most of our structure-function studies on Pattern D M-Prts have been performed on PAM_{AP53} and PAMAP53 fragments (Cnudde et al., 2006; Ringdahl et al., 1998; Ringdahl et al., 1998; Wang et al., 2010a; Wang et al., 2010b), thus allowing facile comparisons with the present work. Amino acid sequence alignments show that these seven PAMs contain similar modular structures and sequence variabilities decrease from the extracellular N-terminus to the C-

terminus, which is closer to the bacterial capsule (Fig. S1). The HVR and A-domains of PAMs, that direct many of their functional properties, are the most diverse regions in the entire protein in terms of their lengths and amino acid sequences. Importantly, because a1- and a2-repeats within the A-domain are the binding loci for hPg, the variabilities in this domain directly relate to the function of PAMs. On the basis of the differences within the A-domain, seven full-length PAMs were categorized into three structural classes in this study (Fig. 1A). Class I contains intact a1- and a2-repeats, each of which harbors one Arg-His dipeptide (simply referred to as RH1 in repeat a1 and RH2 in repeat a2). These RH regions have been shown to be essential residues for hPg binding (Fig. 1B) (Rios-Steiner et al., 2001; Sanderson-Smith et al., 2006b; Schenone et al., 2000; Wang et al., 2010a; Wang et al., 2010b). PAM_{AP53} and PAM_{SS1574}, which are very similar in sequence to each other, were classified as Class I PAMs. Class II PAMs encompassed those lacking the a1-repeat and only containing the single RH2 binding locus in the a2-repeat. These PAMs included $PAM_{NS88.2}$ and PAM_{Ss1448}. Class III PAMs, PAM_{NS223}, PAM_{NS455}, and PAM_{SS1572}, also contained intact a1a2-repeats as shown in Class I, but were interrupted by V-H-D or D-H-D tripeptide insertions at the end of the a1-repeat.

Progressively more limited variability has been observed throughout the B-, C-, D- and Pro/Gly-domains of these PAMs (Fig. S1). It is noteworthy that PAM_{SS1574} is devoid of the third C-repeat, resulting in a significantly smaller protein compared to other PAMs (Fig. S1). Because PAM_{Ss1574} lacks one C-domain, it is possible to generate a fourth class of Pattern D PAMS when considering this aspect of the structure. Our three classifications were based strictly on the a1a2 domains.

3.2 The α-helix is the predominant secondary structure of PAMs

All full-length proteins and truncated peptides were readily purified by affinity chromatography employing the His_6 adduct, as described earlier (Bhattacharya et al., 2014; Chandrahas et al., 2015), and were of high purity as shown by MALDI-TOF, which displayed the values nearly identical to the expected molecular weights (Tables 1, 2).

Despite extensive variations in the N-terminal sequences of PAMS, all full-length proteins displayed overall high α-helix contents, ranging from 30%−70% at 25° C, as determined by Circular Dichroism (CD) measurements. Specifically, α-helices were comprised of ~30% of overall secondary structures in $PAM_{NS88.2}$, PAM_{SS1448}, and PAM_{Ap53}, while PAM_{SS1574} demonstrated a more moderate α-helical content. More strikingly, PAM_{NS223}, PAM_{NS455}, and PAM_{SS1572} contained an α-helical fractional amount of >60% (Fig. 2A, Table 1). Since sequence variabilities progressively decrease from the N- to the C-terminus and the C-D-Pro/Gly domains of PAMs are the most conserved domains, we designed truncated versions at the N-terminus for the prototype PAM_{AP53} to assess the helical contents of the individual regions. The truncated PAMs were constructed from Asn^{42}, the first residue downstream of the signal peptide. The polypeptides, PAM_{AP53_short}, PAM_{AP53_medium}, and PAM_{AP53_long}, extend to Lys^{175} (the beginning of C1-domain), Ala^{207} (the end of the C1-domain), and Lys (the middle of D-domain), respectively (Fig. 1B).

CD spectra of the truncated PAM_{AP53} polypeptides were first obtained using the wavelength scan mode. At 25° C, both PAM_{AP53} and PAM_{AP53_long} showed troughs at 208 nm and 222

nm, a strong signature of α-helix motifs (Fig. 2B). The highest relative percentage of α-helices, at ~50%, was observed from PAM_{AP53_long}, rather than full-length PAM_{AP53}, which has the Pro/Gly helical destabilizing domain at C-terminus (Table 2). Under the same conditions, PAM_{AP53_short} and $PAM_{AP53_}$medium displayed a spectral pattern with a single trough at 208 nm, demonstrating a low propensity of α-helices (Fig. 2B).

The temperature scan mode was then employed to evaluate changes of α-helical content with temperature. For all full-length (Fig. 2C) and truncated (Fig. 2D) r-PAMs, temperature scanning revealed that the mean residue ellipticity (MRE) at 222 nm increased at increasing temperatures, corresponding to a decreased α-helical content. Of note, the MRE values of all the full-length PAMs, together with $PAM_{AP53\_long,}$ showed sigmoidal temperature-dependent curves, while the MRE of PAM_{AP53_short} and PAM_{AP53_medium} increased hyperbolically with temperature changes (Fig. 2C, D).

3.3. The C-repeats mediate the dimerization of PAM

Previous data have shown that PAM_{AP53} exists as a dimer at room temperature (Bhattacharya et al., 2014). Similarly, at 25° C, as shown by molecular weight determinations *via* analytical ultracentrifugation (AUC) (Table 1), all full-length r-PAMs were monodisperse throughout the concentration gradient established at two different rotor speeds and were found to be dimeric (Table 1). On the other hand, the AUC results of truncated r-PAMs demonstrated that PAM_{AP53_short}, with only the HVR, A(a1a2)-, and B-domains, and PAM_{Ap53_medium}, with the HVR-A(a1a2)-B-, and one of three c-repeats (c_1) in the C-domain, were also monodisperse and existed as monomers. PAM_{AP53_long}, extended to contain all three c-repeats in the C-domain and part of the D-domain, dimerized similarly to the full-length r-PAMs (Table 2).

To further reveal the domains essential for dimerization, heptad registers of the amino acid sequences within these seven different PAMs were analyzed and organized according to the classical helical wheel representation (Fig. S2). The Pro/Gly region was not included in these analyses since Pro and Gly would not be expected to exist in helical conformations. Because there are only scattered amino acid substitutions in the three c-repeats and in the D-domain among various naturally occurring PAMs, PAM_{AP53} was chosen as a representative to illustrate the arrangement of amino acids in the helical wheel model of all PAMs (Fig. 3), and to correlate with function-studies accomplished on this PAM_{AP53}. The requisite for such an alignment is a dominance of α-helices and the presence of hydrophobic residues throughout the sequences represented. Optimally, heptad positions *a* and *d* are mainly occupied by Leu and Val residues, and face the inner surfaces in a coiled-coil dimer, while positions *b, c, e, f,* and *g* are exposed to the outer surfaces. The three c-repeats (c1-c3) of all PAMs, except for PAM_{SS1574}, contain a total of 119 residues, rendering the C-domain as the longest of all the PAM domains (Fig. S1). Considering their amino acid compositions, Leu and Val account for over 50% of positions *a* and *d* in the C-domain, thereby providing the opportunity to form hydrophobic clusters in the inner surface of a helical coiled-coil. Additionally, Leu residues were found at positions *a* and *d* in regions of HVRs, as well as A-, B-, and D-domains (Fig. S2), but these domains are shorter than the C-domain. Notably, the typical seven-residue hydrophobic periodicities were interrupted by sequences in a1a2

containing hPg-binding motifs, *viz.,* the Arg-His binding site dipeptides (RH1 and RH2), thus generating flexibility in the α-helices, perhaps providing spacing between the chains for binding of hPg.

Alignments, using heptad registers, were then applied to other domains of PAMs to investigate how the non-polar residues existing in each region form dimers. While highly diverse among PAMs, the HVR also contained some nonpolar residues, *e.g.,* Leu and Val. These residues occupied nearly one-third of positions *a* and *d* in this domain, making it possible to create a portion of a hydrophobic coiled-coil interface (Fig. 4). In this regard, it has been shown that while HVRs of M-Prts from Pattern E strains, viz., M22, M28, and M49, contained even fewer apolar residues at positions *a* and *d* than PAMs, they nonetheless formed canonical dimeric coiled-coils at 4° C (Buffalo et al., 2016), a temperature that stabilized coiled-coil formation. All PAMs, except PAM_{SS1448}, contain a negatively charged cluster in the HVRs at position *c* and/or *g* in the helical wheel. Accordingly, PAM_{SS1448} has a significant higher isoelectric point (pi ~9.3) than the other PAMs (pi ~7.5).

Thus, from the heptad register analyses and the AUC results presented above, we propose that the complete C-domain is essential for PAMs to form stable dimers, confirming an assumption solely based on high sequence conservation for several M-Prts (not of the Pattern D type) (Cedervall et al., 1997; Nilson et al., 1995). Further, hydrophobic residues in other domains can also contribute, albeit to a lesser degree, to the energetics of dimerization. However, it was not known prior to this study whether other highly variable domains could destabilize the C-domain helices. This does not appear to be the case.

3.4. The hPg binding motifs in PAMs readily form mobile loops rather than rigid helices

The homologous a1a2-repeats in PAMs are responsible for binding hPg with very high affinity, and residues in such tandem repeats are not strictly aligned in heptad registers (Fig. S2). Therefore, NMR experiments were performed for three peptides harboring hPg-binding modules (Fig. 5A). Specifically, $AGL55_{NS88.2}$ and $KTI55_{SS1448}$ both originate from the N-terminal region of the HVR of the $PAM_{NS88.2}$ and PAM_{SS1448} (Ala^{95} and Lys^{85}, respectively) to the middle of the B-domain (Y^{149} and Y^{139}, respectively). These two peptides contain a single Arg-His (RH2) motif in the a2 region, due to the natural loss of the a1-repeat in corresponding full-length PAMs. $VEK75_{AP53}$ begins with V^{97} in the HVR region of the N-terminus of PAM_{AP53} and extends to the last residue of B-domain, Q^{171}. This latter peptide contains two Arg-His motifs (RH1 and RH2) present in the a1 and a2 regions, respectively. The MALDI-derived molecular weights of these peptides (Table 2) attest to their high purity. Further, the sedimentation equilibrium data (Table 2) clearly shows that these three peptides exist as monomers in solution and were monodisperse at all points in the concentration gradient at two different rotor speeds. We employed these peptides to determine their 3D structures by NMR in solution to determine how these functional regions are initially conformationally presented to hPg.

Initial NOESY experiments for these peptides show that residues in the N- and C-terminal regions only have sequential connectivities, suggesting a lack of defined secondary structural elements at the termini. Additionally, the $VEK75_{AP53}$ structure presented a long unstructured tail from residue D^{49} to Q^{75} at the C-terminus, corresponding to the majority of

the B-domain (E^{133} to Q^{171}) in PAM_{AP53}. Nonetheless, a significant fraction of α-helical conformations is predicted in the central regions of the peptides based on chemical shifts using TALOS-N and CS-Rosetta (Shen et al., 2010), and confirmed by non-sequential NOEs observed from 2D-NOESY and 3D-NOESY-HSQC experiments. Using the predicated structure from CS-Rosetta as the template, the XPLOR-NIH program was performed to generate structure clusters (Fig. S3) with the lowest energies and without violations in dihedral angle and distance restraints. The structural statistics for each peptide are provided in Table S3. Small average pairwise root mean square derivatives (RMSD) were observed for structured residues indicating that these truncated peptides exist as an ensemble consisting of defined secondary structures. Accordingly, from the ensembles of ten solution structures for AGL55, KTI55, and VEK75, overlaid according to the longest helical structure in each (Fig. S3), the lowest energy structure of each of the three uncomplexed peptides is illustrated in Fig. 5B–D.

In $AGL55_{NS88.2}$, two α-helical segments, from R^8 to E^{24}, and from D^{27} to D^{40}, are connected with a mobile loop consisting of the $R^{25}H^{26}$ dipeptide (Fig. 5B). Similarly, both RH1 and RH2 dipeptides ($R^{17}H^{18}$ and $R^{30}H^{31}$) of VEK75 are also located in mobile loops. Thus, the structures of $AGL55_{NS88.2}$ and $VEK75_{AP53}$ demonstrated flexible hPg-binding modules flanked by rigid helices (Fig. 5B, D). It is noted that the N-terminus of $KTI55_{SS1448}$ contains two short helical segments, and the RH2 dipeptide of $KTI55_{SS1448}$ is situated in a loop region consisting of eight residues (K^{23}-D^{30}) (Fig. 5C). The larger portion of loops upstream of the hPg-binding motif made $KTI55_{SS1448}$ a less compact conformation than the other single-Rî2-containing peptide, AGL55NS88.2. On the basis of solution structures obtained here, we conclude that the RH1 and RH2 hPg-binding motifs readily breach rigid helical structures and become flexible, which likely aids in the binding of hPg. Also, helices are not readily observed in the B-domain of $VEK75_{AP53}$, thereby rendering this region as a mobile structural element (Rios-Steiner et al., 2001; Wang et al., 2010b).

It was also found that in the $AGL55_{NS88.2}$ sequence, oppositely charged residues are staggered every three positions, *i.e.,* Glu^7-Arg^{10}-Glu^{13}-Lys^{16}-Glu^{19}-Arg^{22}. This staggered alignment can stabilize the α-helix through side-chain electrostatic attractions, but such a feature nonetheless is not present in $KTI55_{SS1448}$, rendering this region as less structured than $AGL55_{NS88.2}$.

3.5. r-PAMs demonstrate tight binding to hPg

SPR experiments were next performed to evaluate hPg-binding affinities of the r-PAMs. Class I and III PAMs were similar in their tight binding to hPg, with relatively slow off-rates and resultant K_D values of ~10 nM (Fig. 6 A–E, Table 3). However, two members of C l ass II PAMs somewhat diverged regarding their hPg-binding patterns. Binding of $PAM_{NS88.2}$ to hPg was as strong as Class I and Class III PAMs (Fig. 6F), but PAM_{SS1448} exhibited a K_D of ~30 nM, due to its relatively fast dissociation rate (Fig. 6G, Table 3). But, on the whole, in spite of the variability in a1a2-repeats among different r-PAMs, these dimeric full-length PAMs all tightly associated with hPg with K_D values at the low nM scale. Three truncated variants of Class I PAM, *i.e.,* PAM_{AP53_short}, PAM_{AP53_medium}, and PAM_{AP53_long}, also show tight binding to hPg at the nM scale, suggesting that for PAM_{AP53}, dimerization is not

a determining factor for its binding to hPg, which is consistent with the previous report on this subject (Bhattacharya et al., 2014).

3.6. hPg binding to PAM-containing GAS strains is a measure of surface exposure of PAM

After assuring that all r-PAMS fully bound to hPg, we examined the binding of to the seven PAM-positive GAS cells by flow cytometry in order to assess the PAM protein expression levels on these cell lines. In this assay, the negative control was AP53Δ*pam*. In contrast to the relatively very similar K_d values for hPg to the purified r-PAMs, these GAS strains displayed diversity in their abilities to capture hPg (Fig. 7). SS1574, one of Class I PAM expressing strains, bound the highest amount of hPg, at <2-fold than that of the AP53. Both strains harboring Class II PAMs, *viz.,* NS88.2 and SS1448, associated with hPg at a level comparable to that of AP53. Nevertheless, in Class III PAM-expressing strains, SS1572 only presented a very low constitutive association with hPg, Collectively, we have found that PAM-positive GAS strains diverged in PAM expression, as evaluated by hPg binding.

4. Discussion

The GAS surface-protruding rod-like M-Prt, composed entirely of secondary structure elements, is considered as an essential virulence factor in the pathogenesis of this microbe (Fischetti, 1989; Ghosh, 2011; Smeesters et al., 2010). Recruitment of host proteins to suppress innate immune pathways is a major virulence mechanism of M-Prt and other M-like proteins. Thus, these surface proteins interact with several components of the human host, *e.g.,* hemostasis factors (Loof et al., 2014; Oehmcke et al., 2012), complement inhibitors (Agrahari et al., 2013; Agrahari et al., 2016), and epithelial cell receptors (Frick et al., 2003; Siemens et al., 2011; Tamura and Nittayajarn, 2000), and the great variability of M-Prts in different GAS serotypes allows GAS to display different abilities to colonize and/or invade. Previous research has unveiled structure-function relationships of M-Prts with virulence properties in Pattern A-C and Pattern E strains (Buffalo et al., 2016; Cedervall et al., 1997; Fischetti, 1989; Ghosh, 2011; McNamara et al., 2008; Nilson et al., 1995; Smeesters et al., 2010; Stewart et al., 2016), but more limited research has been accomplished on M-Prts expressed by Pattern D strains. Among the major properties of Pattern D M-Prts (PAMs) is that they serve as the major direct receptors for tight binding to host hPg, a property not shared by other M-Prt pattern types. Genetic linkage of PAM with a specific subtype of SK produced only by Pattern D strains, SK2b, that selectively activates hPg bound to PAM has been established (Zhang et al., 2012). The net result of these interactions is to provide a surface bound protease (hPm) that GAS can employ for release from initially protective fibrin nets and ultimate dissemination via degradation of innate immune barriers. Based on studies with a large peptide region of M1, a M-Prt of the Pattern A-C group which does not directly bind hPg, it is believed that M-Prts exist as parallel kinked coiled-coils with significant exposure of its N-terminal domains on the GAS surface (Buffalo et al., 2016; Ghosh, 2011; McNamara et al., 2008). But, PAMs possess large differences in their hPg binding N-termini (the A-domain, composed of homologous a1a2 repeats) as compared to M1, and do not directly bind to fibrinogen, and secondary structural predictions of the N-termini of PAM do not suggest the presence of stable helical structures. However, studies with isolated r-PAM_{AP53} show that it does, in fact, dimerize (Bhattacharya

et al., 2014). Thus, we have addressed in this report the extent to which the important protein binding N-terminus of PAM stabilizes dimerization of PAM and dictates the tight binding of PAM to hPg.

4.1. Different domains are disparately engaged in PAM dimerization

Three truncated PAM_{AP53} proteins, PAM_{AP53_short}, PAM_{AP53_medium}, and PAM_{AP53_long}, were constructed and expressed (Fig. 1B) to evaluate the contributions to the dimerization of PAM from each domain. The results demonstrated that PAM_{AP53_long}, as a result of containing the three c-repeats in the C-domain, displayed a higher fractional α-helix (49%) than the other two shortened PAM_{AP53} peptides, PAM_{AP53_short} (39%) and PAM_{AP53_medium} (32%), indicating that c-repeats stabilized the α-helical content. PAM_{AP53} (29%), which extended the C-terminus further than PAM_{AP53_long} also contains the Pro/Gly-region, which not unexpectedly disrupted helical structures. PAM_{AP53_short} and PAM_{AP53_medium} demonstrated a transition from partly folded to well-folded peptides at low temperatures (Fig. 2D). These three truncated PAMs demonstrated a transition from partly folded α-helical segments to well-folded dimeric proteins (Fig. 2D). At lower temperatures (4° C), PAM_{AP53_short} and PAM_{AP53_medium} also showed dimerization (C. Q., unpublished data), suggesting that Leu residues in domains upstream of the C-repeats had a propensity to form a hydrophobic core in dimers. However, limited numbers of such residues in a single c-repeat could not facilitate PAM_{AP53_medium} to dimerize at 25° C, whereas PAM_{AP53_long}, incorporating three intact C-repeats, exhibited complete and stable dimerization at 25° C. This implies that the length of C-repeats dominates the balance between monomer and dimer.

In this investigation, it is shown that naturally occurring pAMs from seven different GAS strains are dimeric without exception, as shown by AUC experiments at 25° C (Table 2). Related conclusions can be made from CD temperature scan spectra. The MREs of all the full-length pAMs, as well as pAM_{Ap53_long}, increased sigmoidally as the temperatures were increased, reminiscent of cooperative transitions of DNA melting curves with disruption of helical stacking occurred followed by disruption of the dimeric structures. Thus, these CD results suggested that coiled-coil dimerization is a key feature of those pAMs that harbor intact c-repeats. In contrast, PAM_{AP53_short} and PAM_{AP53_medium} displayed hyperbolic shapes in their melting curves, indicating that helical disruption, but not dissociation, occurred as a function of temperature, which probably preceded dissociation. These hyperbolic melting patterns support the AUC data showing that these latter two peptides existed as monomers at 25° C.

Previous work has demonstrated that the B-domain of M1, from Pattern A-C strains, contain residues that disrupted segments of the coiled-coil helices, allowing kinks in the helices that are important in the binding of M1 to fibrinogen (McNamara et al., 2008). Further, the B-domain of Pattern A-C M6 protein show interruptions in the seven-residue periodicity, thus making this region more flexible (Fischetti et al., 1988). Whether PAMs form kinked dimers to allow hPg binding is not known. However, the NMR studies indicated that an extensive mobile loop in the B-domain has been observed from solution structure of $VEK75_{AP53}$, suggesting that this region is predominantly unstructured in the unbound form. If rigid

helical structures predominated in the B-domain, recruitment of the large hPg, *via* a1a2-repeats, would require conformational changes, possibly destabilizing the coiled-coil dimer at the adjacent C-repeats. In this sense, the B-domain can serve as a cushion to release potential torsional forces generated from association of PAMs with hPg.

It is clear that the c-repeats are the major contributors to the coiled-coil dimerization of PAM. In this region, Leu and Val residues from two helical chains generate a hydrophobic core to stabilize the dimeric conformation. On the other hand, Arg and Lys residues are scattered along C-domain, which would destabilize dimerization through electrostatic repulsions. However, it has been demonstrated that the alkyl group of Arg^{39} in the protein, C4BPa1, contributed to a hydrophobic nook and clustered with apolar side chains in the HVRs of M2, M22, M28, and M49 proteins (Buffalo et al., 2016). While, in the case of PAMs, the HVR does not bind to C4BPa1 (Agrahari et al., 2013), we can nonetheless infer that in PAM c-repeats, the Lys and Arg residues at positions *a* and *d* in the heptads have the potential to produce an internal hydrophobic niche through their alkyl groups. Once the inner hydrophobic core forms, most of the charged residues align at the solvent surface (*i.e.,* positions *b, c, e, f,* and *g* in the heptad). Of importance, positions *a* and *e* of the heptads are mainly occupied by positively charged residues, while predominant amino acids of position *g* are negatively charged Asp or Glu, which are positioned to provide charge attractions.

4.2. A model of PAM structures

We herein propose a secondary structural model to describe the dimerization pattern for PAMs (Fig. 8). Based upon AUC results and the helical wheel modeling, the C-domain has been shown to be the most important region for dimer formation, and hence proposed as the hinge part of the model. To a lesser extent, the D-domain and HVR contribute to dimerization. Contrarily, the α-helices of the a1a2-repeats of the A-domain in different PAMs are disrupted by the hPg binding Arg-His motifs, upstream of the B-domain, which mainly consists of mobile loops. Accordingly, these two coiled-coil destabilizing domains constitute separated concave rings in the illustrated model.

It has been shown that coiled-coil oligomers exist in proteins in both eukaryotes and prokaryotes, *e.g.,* tropomyosin (Sodek et al., 1972) and tropocollagen (Bianchi et al., 1966). It has also been reported that the minimum length of a chemically synthesized polyheptapeptide, Ac-(Lys-Leu-Glu-Ala-Leu-Glu-Gly)$_n$-Lys-amide, required for the coiled-coil dimerization, was 29 residues (Lau et al., 1984). It therefore seems plausible for bacteria to synthesize such polyheptapeptides only up to 30–40 residues when they express dimeric surface virulence factors, such as PAMs. Thus, the polar or charged residues, which are substituted for Leu, Ile, or Val at positions *a* and *d* in heptad registers, interrupt the coiled-coil oligomer. Therefore, to accomplish the formation of functional PAM dimers in solution, GAS strains synthesize significantly more amino acids in each chain at the expense of energy. This strategy encompasses the long dimeric C-domain, together with the D-domain, to maintain a1a2-repeats distant from the cell surface, which would otherwise interfere with binding of PAMs to hPg and other proteins.

Next, residues at position *a* and *d* in heptad registers, other than Leu or Val, may function to create a hydrophilic niche, especially at higher temperatures. In this case, the aliphatic side

chains of Leu or Val residues are exposed to an aqueous environment, and the potential of a rod-like conformation would be high. It is thus suggested that to achieve the most energetically favorable format, the hydrophilic heads of Lys, Arg, and Ser of the C-domain become coiled-coil destabilizing residues and interact with the aqueous environment to retain the apolar environment in the interior.

4.3. Regulation of PAM expression in different GAS strains

Although it has been reported that hPg binds to streptococcal enolase and GAPDH, metabolically necessary enzymes present in all GAS strains (Pancholi and Fischetti, 1998; Winram and Lottenberg, 1996), the binding affinities of hPg to these receptors are much weaker than that of PAM. Because all naturally occurring PAMs bind to hPg with similar affinities at 25° C, divergence in whole-cell binding among pam-positive GAS strains will depend on the PAM expression levels on the cell surface. Thus, hPg binding to Pattern D GAS cells is a determinant for the integrity of PAM on these same cells.

5. Conclusions

The significance of this study is the proposal of an experimentally-based model that depicts the dimerization of PAMs. Biophysical methods were employed to reveal the manner in which dimerization of PAMs has occurred, mainly stabilized by the C-domain with three c-repeats. The HVR and D-domain are also engaged to a lesser extent in the stabilization of PAM dimers. Coiled-coil disrupting regions, including the a1a2 repeats and the B-domain, are relevant to allow high affinity binding of PAMs to hPg.

From the evolutionary perspective, it is necessary for GAS to develop a strategy that permits synthesis of a long rod-like region of PAM, which maintains the functionally-relevant N-terminus distant from the cell surface. On the other hand, charged or polar residues at positions *a* and *d* in the C-repeats, which seemingly destabilize coiled-coil dimerization, provide PAMs and GAS cells with the ability to remain well-tuned to the higher temperatures in which they operate.

Supplementary Material

Refer to Web version on PubMed Central for supplementary material.

Acknowledgments

Funding

This work was supported by NIH Grant HL013423.

References

Agrahari G, Liang Z, Mayfield JA, Balsara RD, Ploplis VA, Castellino FJ, 2013 Complement-mediated opsonization of invasive Group A Streptococcus pyogenes strain AP53 is regulated by the bacterial two-component cluster of virulence responder/sensor (CovRS) system. J. Biol. Chem 288, 27494–27504. [PubMed: 23928307]

Agrahari G, Liang Z, Glinton K, Lee SW, Ploplis VA, Castellino FJ, 2016 Streptococcus pyogenes employs strain-dependent mechanisms of C3b inactivation to inhibit phagocytosis and killing of bacteria. J. Biol. Chem 291, 9181–9189. [PubMed: 26945067]

Babul J, Stellwagen E, 1969 Measurement of protein concentration with interferences optics. Anal. Biochem 28, 216–221. [PubMed: 5781411]

Bao Y, Liang Z, Booyjzsen C, Mayfield JA, Li Y, Lee SW, Ploplis VA, Song H, Castellino FJ, 2014 Unique genomic arrangements in an invasive serotype M23 strain of Streptococcus pyogenes identify genes that induce hypervirulence. J. Bacteriol 196, 4089–4102. [PubMed: 25225265]

Beall B, Facklam R, Thompson T, 1996 Sequencing emm-specific PCR products for routine and accurate typing of group A streptococci. J. Clin. Microbiol 34, 953–958. [PubMed: 8815115]

Berge A, Sjobring U, 1993 PAM, a novel plasminogen-binding protein from Streptococcus pyogenes. J. Biol. Chem 268, 25417–25424. [PubMed: 8244975]

Berge A, Bjorck L, 1995 Streptococcal cysteine proteinase releases biologically active fragments of streptococcal surface proteins. J. Biol. Chem 270, 9862–9870. [PubMed: 7730368]

Berggard K, Johnsson E, Morfeldt E, Persson J, Stalhammar-Carlemalm M, Lindahl G, 2001 Binding of human C4BP to the hypervariable region of M protein: a molecular mechanism of phagocytosis resistance in Streptococcus pyogenes. Mol. Microbiol 42, 539–551. [PubMed: 11703674]

Bessen DE, 2016 Molecular basis of serotyping and the underlying genetic organization of Streptococcus pyogenes. In: Streptococcus pyogenes: Basic Biology to Clinical Manifestations (Ferretti JJ, Stevens DL, Fischetti VA), editors.

Bessen DE, Sotir CM, Readdy TL, Hollingshead SK, 1996 Genetic correlates of throat and skin isolates of group A streptococci. J. Infect. Dis 173, 896–900. [PubMed: 8603968]

Bhattacharya A, Tejero R, Montelione GT, 2007 Evaluating protein structures determined by structural genomics consortia. Proteins 66, 778–795. [PubMed: 17186527]

Bhattacharya S, Liang Z, Quek AJ, Ploplis VA, Law R, Castellino F,J, 2014 Dimerization is not a determining factor for functional high affinity human plasminogen binding by the group A streptococcal virulence factor PAM and is mediated by specific residues within the PAM a1a2 domain. J. Biol. Chem 289, 21684–21693. [PubMed: 24962580]

Bianchi E, Conio G, Ciferri A, 1966 The helix-coil transformation for tropocollagen solutions and its relationship to transformations involving the crystalline form of the protein. Biopolymers 4, 957–970. [PubMed: 5927648]

Buffalo C, Bahn-Suh AJ, Hirakis SP, Biswas T, Amaro RE, Nizet V, Ghosh P, 2016 Conserved patterns hidden within group A Streptococcus M protein hypervariability recognize human C4b-binding protein. Nat. Microbiol 1, 16155. [PubMed: 27595425]

Cedervall T, Johansson MU, Akerstrom B, 1997 Coiled-coil structure of group A streptococcal M proteins. Different temperature stability of class A and C proteins by hydrophobic-nonhydrophobic amino acid substitutions at heptad positions a and d. Biochemistry 36, 4987–4994. [PubMed: 9125521]

Chandrahas V, Glinton K, Liang Z, Donahue DL, Ploplis VA, Castellino FJ, 2015 Direct host plasminogen binding to bacterial surface M-protein in Pattern D strains of Streptococcus pyogenes Is required for activation by Its natural coinherited SK2b protein. J. Biol. Chem 290, 18833–18842. [PubMed: 26070561]

Chen YH, Yang JT, Martinez HM, 1972 Determination of the secondary structures of proteins by circular dichroism and optical rotatory dispersion. Biochemistry 11, 4120–4131. [PubMed: 4343790]

Clubb RT, Thanabal V, Wagner G, 1992 A constant-time 3-dimensional triple-resonance pulse scheme to correlate intraresidue H-1(N), N-15, and C-13(‘) chemical-shifts in N-15-C-13-labeled proteins. J. Magn. Reson. 97, 213–217.

Cnudde SE, Prorok M, Castellino FJ, Geiger JH, 2006 X-ray crystallographic structure of the angiogenesis inhibitor, angiostatin, bound to a peptide from the group A streptococcal surface protein PAM. Biochemistry 45, 11052–11060. [PubMed: 16964966]

Fischetti VA, 1989 Streptococcal M protein: molecular design and biological behavior. Clin. Microbiol. Rev 2, 285–314. [PubMed: 2670192]

Fischetti VA, 1991 Streptococcal M protein. Sci. Am 264, 58–65. [PubMed: 1857955]

Fischetti VA, Parry DA, Trus BL, Hollingshead SK, Scott JR, Manjula BN, 1988 Conformational characteristics of the complete sequence of group A streptococcal M6 protein. Proteins 3, 60–69. [PubMed: 3287371]

Frick IM, Schmidtchen A, Sjobring U, 2003 Interactions between M proteins of Streptococcus pyogenes and glycosaminoglycans promote bacterial adhesion to host cells. Eur. J. Biochem 270, 2303–2311. [PubMed: 12752450]

Ghosh P, 2011 The nonideal coiled coil of M protein and its multifarious functions in pathogenesis. Adv. Exp. Med. Biol 715, 197–211. [PubMed: 21557065]

Ghosh P, 2018 Variation, indispensability, and masking in the M protein. Trends Microbiol. 26, 132–144. [PubMed: 28867148]

Glinton K, Beck J, Liang Z, Qiu C, Lee SW, Ploplis VA, Castellino FJ, 2017 Variable region in streptococcal M-proteins provides stable binding with host fibrinogen for plasminogen-mediated bacterial invasion. J. Biol. Chem 292, 6775–6785. [PubMed: 28280245]

Greenfield NJ, 2006 Analysis of the kinetics of folding of proteins and peptides using circular dichroism. Nat. Protoc 1, 2891–2899. [PubMed: 17406548]

Gustafsson MCU, Lannergård J, Nilsson OR, Kristensen BM, Olsen JE, Harris CL, Ufret-Vincenty RL, Stålhammar-Carlemalm M, Lindahl G, 2013 Factor H binds to the hypervariable region of many streptococcus pyogenes M proteins but does not promote phagocytosis resistance or acute virulence. PLoS Pathog. 9, e1003323. [PubMed: 23637608]

Herwald H, Cramer H, Morgelin M, Russell W, Sollenberg U, Norrby-Teglund A, Flodgaard H, Lindbom L, Bjorck L, 2004 M protein, a classical bacterial virulence determinant, forms complexes with fibrinogen that induce vascular leakage. Cell 116, 367–379. [PubMed: 15016372]

Hollingshead SK, Fischetti VA, Scott JR, 1986 Complete nucleotide sequence of type 6 M protein of the group A Streptococcus. Repetitive structure and membrane anchor. J. Biol. Chem 261, 1677–1686. [PubMed: 3511046]

Hondorp ER, McIver KS, 2007 The Mga virulence regulon: infection where the grass is greener. Mol. Microbiol 66, 1056–1065. [PubMed: 18001346]

Ikura M, Kay LE, Tschudin R, Bax A, 1990 3-Dimensional NOESY-HMQC spectroscopy of a C-13-labeled protein. J. Magn. Reson 86, 204–209.

Kay L, Keifer P, Saarinen T, 1992 Pure absorption gradient enhanced heteronuclear single quantum correlation spectroscopy with improved sensitivity. J. Am. Chem. Soc 114, 10663–10665.

Kay LE, Ikura M, Tschudin R, Bax A, 2011 Three-dimensional triple-resonance NMR spectroscopy of isotopically enriched proteins. 1990. J. Magn. Reson 213, 423–441. [PubMed: 22152361]

Lahteenmaki K, Kuusela P, Korhonen TK, 2001 Bacterial plasminogen activators and receptors. FEMS Microbiol. Rev 25, 531–552. [PubMed: 11742690]

Laskowski RA, MacArthur MW, Moss DS, Thornton JM, 1993 PROCHEK: a program to check the stereochemical quality of protein structures. J. Appl. Cryst 26, 283–291.

Lau SY, Taneja AK, Hodges RS, 1984 Synthesis of a model protein of defined secondary and quaternary structure. Effect of chain length on the stabilization and formation of two-stranded alpha-helical coiled-coils. J. Biol. Chem 259, 13253–13261. [PubMed: 6490655]

Lee JL, Naguwa SM, Cheema GS, Gershwin ME, 2009a Acute rheumatic fever and its consequences: a persistent threat to developing nations in the 21st century. Autoimmun. Rev 9, 117–123. [PubMed: 19386288]

Lee W, Westler WM, Bahrami A, Eghbalnia HR, Markley JL, 2009b PINE-SPARKY: graphical interface for evaluating automated probabilistic peak assignments in protein NMR spectroscopy. Bioinformatics 25, 2085–2087. [PubMed: 19497931]

Liang Z, Zhang Y, Agrahari G, Chandrahas V, Glinton K, Donahue DL, Balsara RD, Ploplis VA, Castellino FJ, 2013 A natural inactivating mutation in the CovS component of the CovRS regulatory operon in a pattern D Streptococcal pyogenes strain influences virulence-associated genes. J. Biol. Chem 288, 6561–6573. [PubMed: 23316057]

Lohr F, Ruterjans H, 2002 Correlation of backbone amide and side-chain 13C resonances in perdeuterated proteins. J. Magn. Reson 156, 10–18. [PubMed: 12081438]

Loof TG, Deicke C, Medina E, 2014 The role of coagulation/fibrinolysis during Streptococcus pyogenes infection. Frontiers in cellular and infection microbiology 4, 128. [PubMed: 25309880]

Markley JL, Bax A, Arata Y, Hilbers CW, Kaptein R, Sykes BD, Wright PE, Wuthrich K, 1998 Recommendations for the presentation of NMR structures of proteins and nucleic acids. IUPAC-IUBMB-IUPAB Inter-Union Task Group on the Standardization of Data Bases of Protein and Nucleic Acid Structures Determined by NMR Spectroscopy. J. Biomol. NMR 12, 1–23. [PubMed: 9729785]

Mason JM, K MM, Arndt KM, 2008 iPEP: peptides designed and selected for interfering with protein interaction and function. Biochem. Soc. Trans 36, 1442–1447. [PubMed: 19021572]

McIver KS, Scott JR, 1997 Role of mga in growth phase regulation of virulence genes of the group A streptococcus. J. Bacteriol 179, 5178–5187. [PubMed: 9260962]

McIver KS, Heath AS, Green BD, Scott JR, 1995 Specific binding of the activator Mga to promoter sequences of the emm and scpA genes in the group A streptococcus. J. Bacteriol 177, 661906624.

McNamara C, Zinkernagel AS, Macheboeuf P, Cunningham MW, Nizet V, Ghosh P, 2008 Coiled-coil irregularities and instabilities in group A Streptococcus M1 are required for virulence. Science 319, 1405–1408. [PubMed: 18323455]

McNeilly CL, McMillan DJ, 2014 Horizontal gene transfer and recombination in Streptococcus dysgalactiae subsp. equisimilis. Front. Microbiol. 5, 676. [PubMed: 25566202]

Mori S, Abeygunawardana C, Johnson MO, van Zijl PC, 1995 Improved sensitivity of HSQC spectra of exchanging protons at short interscan delays using a new fast HSQC (FHSQC) detection scheme that avoids water saturation. J. Magn. Reson. B 108, 94–98. [PubMed: 7627436]

Nilson BH, Frick IM, Akesson P, Forsen S, Bjorck L, Akerstrom B, Wikstrom M, 1995 Structure and stability of protein H and the Ml protein from Streptococcus pyogenes. Implications for other surface proteins of gram-positive bacteria. Biochemistry 34, 13688–13698. [PubMed: 7577960]

Oehmcke S, Morgelin M, Malmstrom J, Linder A, Chew M, Thorlacius H, Herwald H, 2012 Stimulation of blood mononuclear cells with bacterial virulence factors leads to the release of pro-coagulant and pro-inflammatory microparticles. Cell. Microbiol 14, 107–119. [PubMed: 21951918]

Pancholi V, Fischetti VA, 1998 alpha-enolase, a novel strong plasmin(ogen) binding protein on the surface of pathogenic streptococci. J. Biol. Chem 273, 14503–14515. [PubMed: 9603964]

Phillips GN, Flicker PF, Cohen C, Manjula BN, Fischetti VA, 1981 Streptococcal M protein: alpha-helical coiled-coil structure and arrangement on the cell surface. Proc. Natl. Acad. Sci. USA 78, 4689–4993. [PubMed: 7029524]

Ringdahl U, Svensson M, Wistedt AC, Renn T, Kellner R, Muller-Esterl W, Sjobring U, 1998 Molecular co-operation between protein PAM and streptokinase for plasmin acquisition by Streptococcus pyogenes. J. Biol. Chem 272, 6424–6230.

Rios-Steiner JL, Schenone M, Mochalkin I, Tulinsky A, Castellino FJ, 2001 Structure and binding determinants of the recombinant kringle-2 domain of human plasminogen to an internal peptide from a group A Streptococcal surface protein. J. Mol. Biol 308, 705–719. [PubMed: 11350170]

Sanderson-Smith M, Batzloff M, Sriprakash KS, Dowton M, Ranson M, Walker MJ, 2006a Divergence in the plasminogen-binding group a streptococcal M protein family: functional conservation of binding site and potential role for immune selection of variants. J. Biol. Chem 281, 3217–3226. [PubMed: 16319056]

Sanderson-Smith ML, Walker MJ, Ranson M, 2006b The maintenance of high affinity plasminogen binding by group A streptococcal plasminogen-binding M-like protein is mediated by arginine and histidine residues within the a1 and a2 repeat domains. J. Biol. Chem 281, 25965–25971. [PubMed: 16822869]

Sanderson-Smith ML, Dowton M, Ranson M, Walker MJ, 2007 The plasminogen-binding group A streptococcal M protein-related protein Prp binds plasminogen via arginine and histidine residues. J. Bacteriol 189, 1435–1440. [PubMed: 17012384]

Sanderson-Smith ML, Dinkla K, Cole JN, Cork AJ, Maamary PG, McArthur JD, Chhatwal GS, Walker MJ, 2008 M protein-mediated plasminogen binding is essential for the virulence of an invasive Streptococcus pyogenes isolate. FASEB J. 22, 2715–2722. [PubMed: 18467595]

Schenone MM, Warder SE, Martin JA, Prorok M, Castellino FJ, 2000 An internal histidine residue from the bacterial surface protein, PAM, mediates its binding to the kringle-2 domain of human plasminogen. J. Pept. Res 56, 438–445. [PubMed: 11152303]

Schiffer M, Edmundson AB, 1967 Use of helical wheels to represent the structures of proteins and to identify segments with helical potential. Biophys. J 7, 121–135. [PubMed: 6048867]

Schuck P, Gillis RB, Besong TM, Almutairi F, Adams GG, Rowe AJ, Harding SE, 2014 SEDFIT-MSTAR: molecular weight and molecular weight distribution analysis of polymers by sedimentation equilibrium in the ultracentrifuge. Analyst 139, 79–92. [PubMed: 24244936]

Schwieters CD, Kuszewski JJ, Clore GM, 2006 Using Xplor-NIH for NMR molecular structure determination. Prog. Nucl. Mag. Res. Sp 48, 47–62.

Schwieters CD, Bermejo GA, Clore GM, 2018 Xplor-NIH for molecular structure determination from NMR and other data sources. Protein Sci. 27, 26–40. [PubMed: 28766807]

Schwieters CD, Kuszewski JJ, Tjandra N, Clore GM, 2003 The Xplor-NIH NMR molecular structure determination package. J. Magn. Reson 160, 65–73. [PubMed: 12565051]

Shen Y, Bax A, 2013 Protein backbone and sidechain torsion angles predicted from NMR chemical shifts using artificial neural networks. J. Biomol. NMR 56, 227–241. [PubMed: 23728592]

Shen Y, Delaglio F, Cornilescu G, Bax A, 2009 TALOS plus : a hybrid method for predicting protein backbone torsion angles from NMR chemical shifts. J. Biomol. NMR 44, 213–223. [PubMed: 19548092]

Shen Y, Bryan PN, He Y, Orban J, Baker D, Bax A, 2010 De novo structure generation using chemical shifts for proteins with high-sequence identity but different folds. Protein Sci. 19, 349–356. [PubMed: 19998407]

Shen Y, Lange O, Delaglio F, Rossi P, Aramini JM, Liu G, Eletsky A, Wu Y, Singarapu KK, Lemak A, Ignatchenko A, Arrowsmith CH, Szyperski T, Montelione GT, Baker DM, Bax A, 2008 Consistent blind protein structure generation from NMR chemical shift data. Proc. Natl. Acad. Sci. USA 105, 4685–4690. [PubMed: 18326625]

Siemens N, Patenge N, Otto J, Fiedler T, Kreikemeyer B, 2011 Streptococcus pyogenes M49 plasminogen/plasmin binding facilitates keratinocyte invasion via integrin-integrin linked kinase (ILK) pathways and protects from macrophage killing. J. Biol. Chem 286, 21612–21622. [PubMed: 21521694]

Smeesters PR, McMillan DJ, Sriprakash KS, 2010 The streptococcal M protein: a highly versatile molecule. Trends Microbiol. 18, 275–282. [PubMed: 20347595]

Sodek J, Hodges RS, Smillie LB, Jurasek L, 1972 Amino-acid sequence of rabbit skeletal tropomyosin and its coiled-coil structure. Proc. Natl. Acad. Sci. USA 69, 3800–3804. [PubMed: 4509342]

Stewart CM, Buffalo CZ, Valderrama JA, Henningham A, Cole JN, Nizet V, Ghosh P, 2016 Coiled-coil destabilizing residues in the group A Streptococcus M1 protein are required for functional interaction. Proc. Natl. Acad. Sci. USA 113, 9515–9520. [PubMed: 27512043]

Sumitomo T, Nakata M, Higashino M, Yamaguchi M, Kawabata S, 2016 Group A Streptococcus exploits human plasminogen for bacterial translocation across epithelial barrier via tricellular tight junctions. Sci Rep 7, 20069. [PubMed: 26822058]

Sun H, Ringdahl U, Homeister JW, Fay WP, Engelberg NC, Yang AY, Rozek LS, Wang X, Sjobring U, Ginsburg D, 2004 Plasminogen is a critical host pathogenicity factor for Group A streptococcal infection. Science 305, 1283–1286. [PubMed: 15333838]

Talluri S, Wagner G, 1996 An optimized 3D NOESY-HSQC. J. Magn. Reson 112, 200–205.

Tamura GS, Nittayajarn A, 2000 Group B streptococci and other gram-positive cocci bind to cytokeratin 8. Infect. Immun. 68, 2129–2134. [PubMed: 10722610]

Walker MJ, Barnett TC, McArthur JD, Cole JN, Gillen CM, Henningham A, Sriprakash KS, Sanderson-Smith ML, Nizet V, 2014 Disease manifestations and pathogenic mechanisms of group A Streptococcus. Clin. Microbiol. Rev 27, 264–301. [PubMed: 24696436]

Wang M, Prorok M, Castellino FJ, 2010a NMR backbone dynamics of VEK-30 bound to the human plasminogen kringle 2 domain. Biophys. J 99, 302–312. [PubMed: 20655859]

Wang M, Zajicek J, Geiger JH, Prorok M, Castellino FJ, 2010b Solution structure of the complex of VEK-30 and plasminogen kringle 2. J. Struct. Biol 169, 349–359. [PubMed: 19800007]

Ward PN, Leigh JA, 2002 Characterization of PauB, a novel broad-spectrum plasminogen activator from Streptococcus uberis. J. Bacteriol. 184, 119–125. [PubMed: 11741851]

Winram SB, Lottenberg R, 1996 The plasmin-binding protein Plr of group A streptococci is identified as glyceraldehyde-3-phosphate dehydrogenase. Microbiology 142, 2311–2320. [PubMed: 8760943]

Wistedt AC, Ringdahl U, Mulleresterl W, Sjobring U, 1995 Identification of a plasminogen-binding motif in PAM, a bacterial surface protein. Mol. Microbiol 18, 569–578. [PubMed: 8748039]

Wittekind M, Mueller L, 1993 HNCACB, A high-sensitivity 3D NMR experiment to correlate amide-proton and nitrogen resonances with the alpha-carbon and beta-carbon resonances in proteins. J. Magn. Reson 101, 201–205.

Wong AP, Cortez SL, Baricos WH, 1992 Role of plasmin and gelatinase in extracellular matrix degradation by cultured rat mesangial cells. Am. J. Physiol 236, F1112–F1118.

Yuan Y, Zajicek J, Qiu C, Chandrahas V, Lee SW, Ploplis VA, Castellino FJ, 2017 Conformationally organized lysine isosteres in Streptococcus pyogenes M protein mediate direct high-affinity binding to human plasminogen. J. Biol. Chem 292, 15016–15027. [PubMed: 28724633]

Zhang Y, Liang Z, Hsueh HT, Ploplis VA, Castellino FJ, 2012 Characterization of streptokinases from Group A streptococci reveals a strong functional relationship that supports the coinheritance of plasminogen-binding M-Protein and cluster 2b streptokinase. J. Biol. Chem 287, 42093–42103. [PubMed: 23086939]

Zhang Y, Liang Z, Glinton K, Ploplis VA, Castellino FJ, 2013 Functional differences between Streptococcus pyogenes cluster 1 and cluster 2b streptokinases are determined by their β-domains. FEBS Lett. 587, 1304–1309. [PubMed: 23474243]

Highlights

- Group A *S. pyogenes* (GAS) is a causative agent in pharyngeal and dermal infections.
- A major virulence determinant of GAS is the signature dimeric modular M-protein.
- Host human plasminogen binds to the A-domain of all Pattern D M-proteins and governs virulence.
- The determinants of Pattern D M-protein dimerization reside in its helical C-domain.
- The modular nature of M-proteins are evolutionarily designed for bacterial survival in hostile host niches.

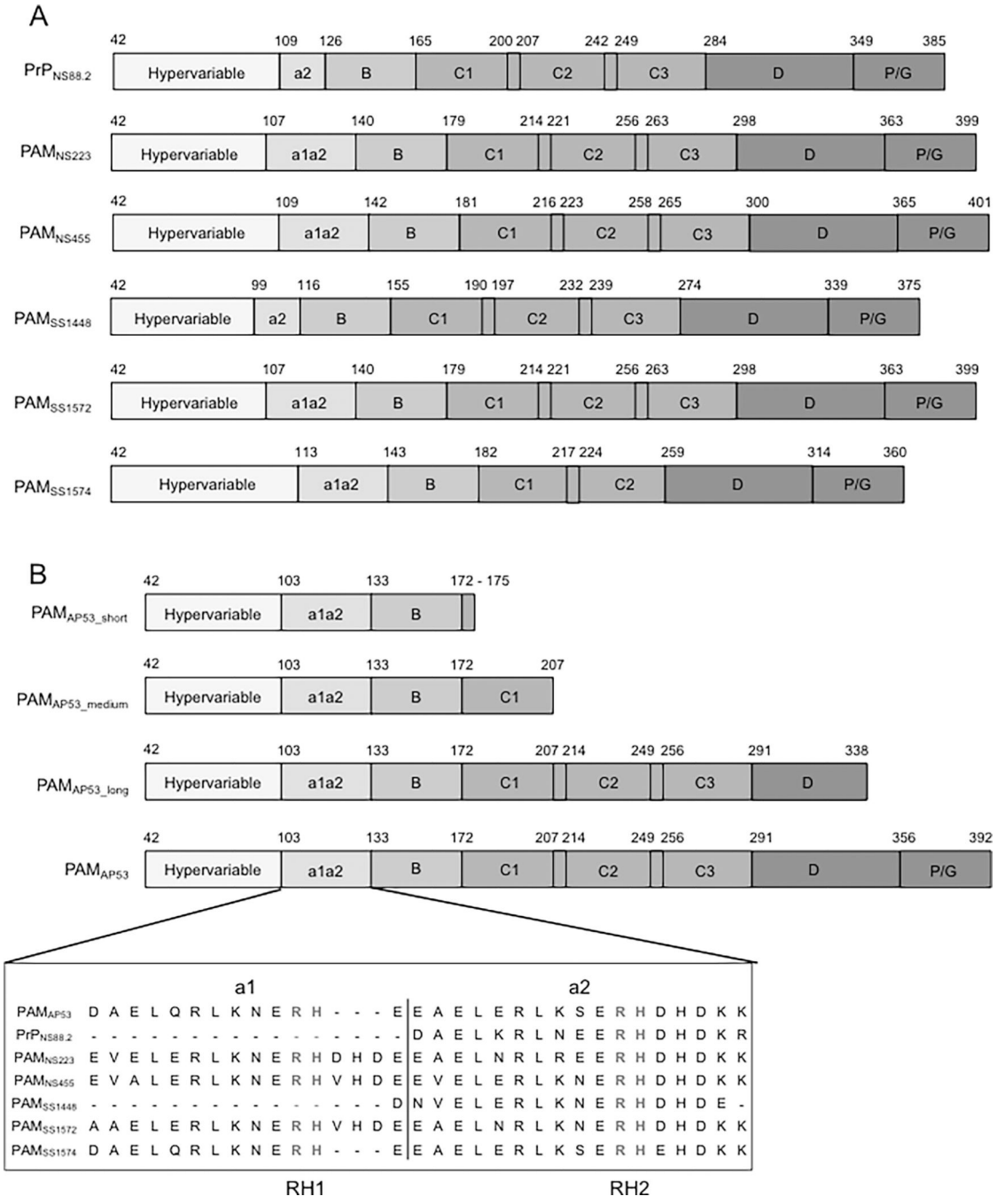

Fig. 1.

Schematics of full-length r-PAMs and truncated r-PAM_{AP53} peptides. All recombinant proteins start with the first residue (#42) immediately after the signal peptide. (A) Within all naturally occurring PAMs, homology progressively increases from their N- to C-termini. Domains align in the following order from the N-terminus: hypervariable region (HVR), A-domai n containing a1a2- or a2-repeats, B-domain, C-domain containing c1-c3 repeats, D-domain, and the Pro/Gly (P/G)-rich region. (B) Three truncated PAM_{AP53} proteins were prepared that terminated at different locations in the PAM_{AP53} sequence. The a1a2-repeats

are zoomed in to manifest the variability of this domain among different r-PAMs. Residues in red refer to the sequence of a1a2-repeats, and residues in blue indicate the Arg-His (RH) motifs that specifically binding to hPg (Rios-Steiner et al., 2001; Sanderson-Smith et al., 2006b; Schenone et al., 2000; Wang et al., 2010a; Wang et al., 2010b). Dashes are applied to increase the homology of alignment when necessary. The schematic is drawn to relative scale, and numbers indicate the first and last residue of each domain.

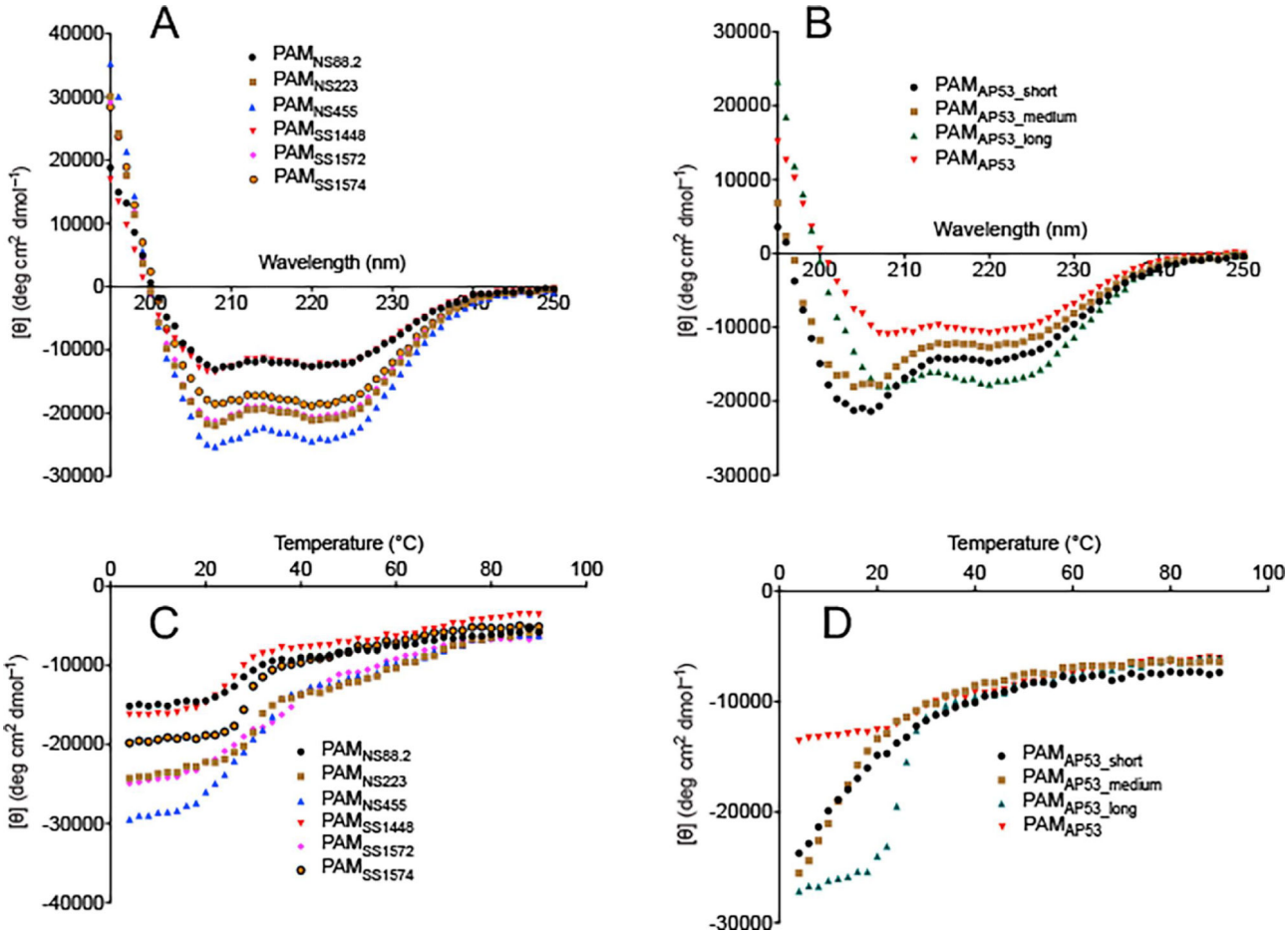

Fig. 2.

CD spectra of naturally occurring r-PAMs and truncated r-PAM$_{Ap53}$ peptides. Mean residue ellipticities (MRE) of each protein and peptide were calculated from their CD signals. The MRE is plotted as a function of wavelength from 195 nm to 250 nm at 25° C (A and B), and as a function of temperature from 4° C to 90° C at 222 nm (C and D). The results are shown as data points that represent the average of triplicate scans at a given wavelength or temperature.

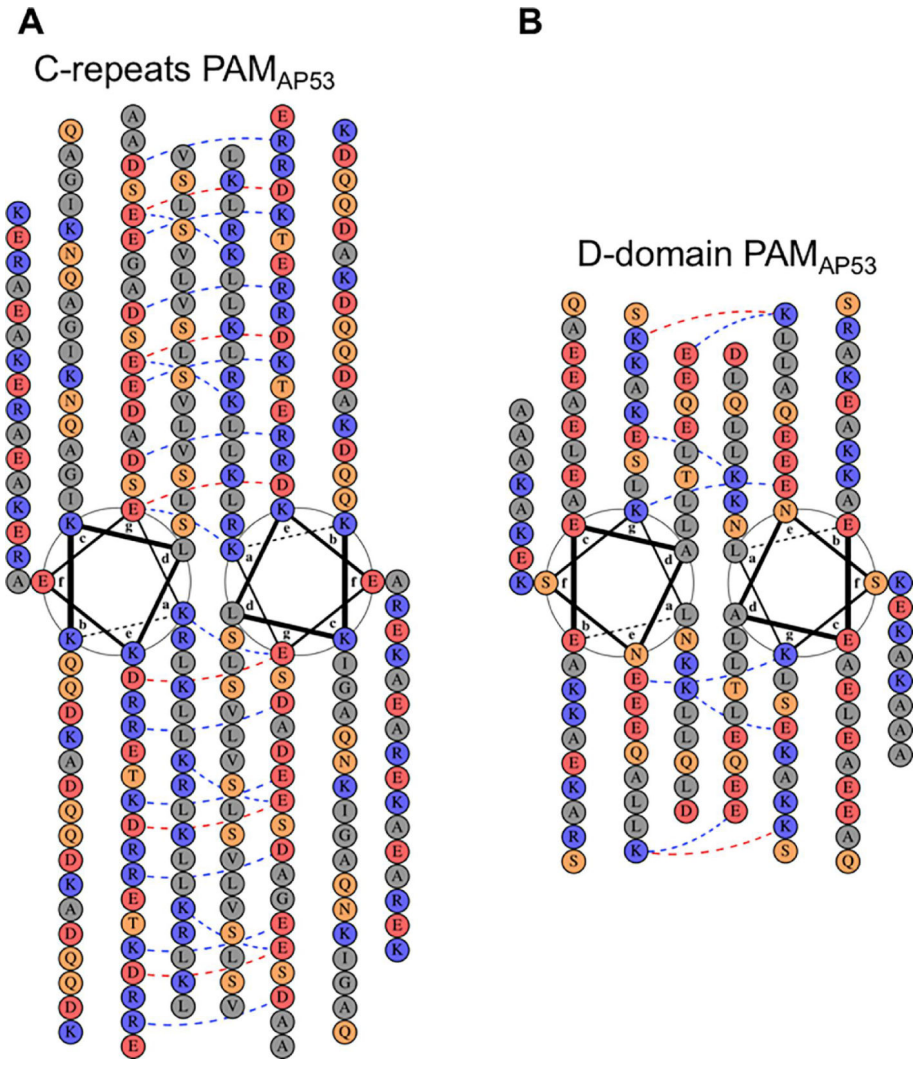

Fig. 3.

Helical wheel representations of the highly conserved C- and D-domains of PAM$_{Ap53}$. Construction of helical wheels for (A) c1-c3 repeats of the C-domain and (B) the D-domain was performed on the server, DrawCoil 1.0 (http://www.grigoryanlab.org/drawcoil/). The position of each residue is identical to that from the heptad register alignment (Fig. S2). Residues are categorized and highlighted in colored circles: grey, apolar residues; blue, positively charged residues; red, negatively charged residues; orange, polar residues. The blue and red dash lines indicate potential electrostatic attractions and repulsions, respectively, between residues at positions *e* and *g* (Mason et al., 2008).

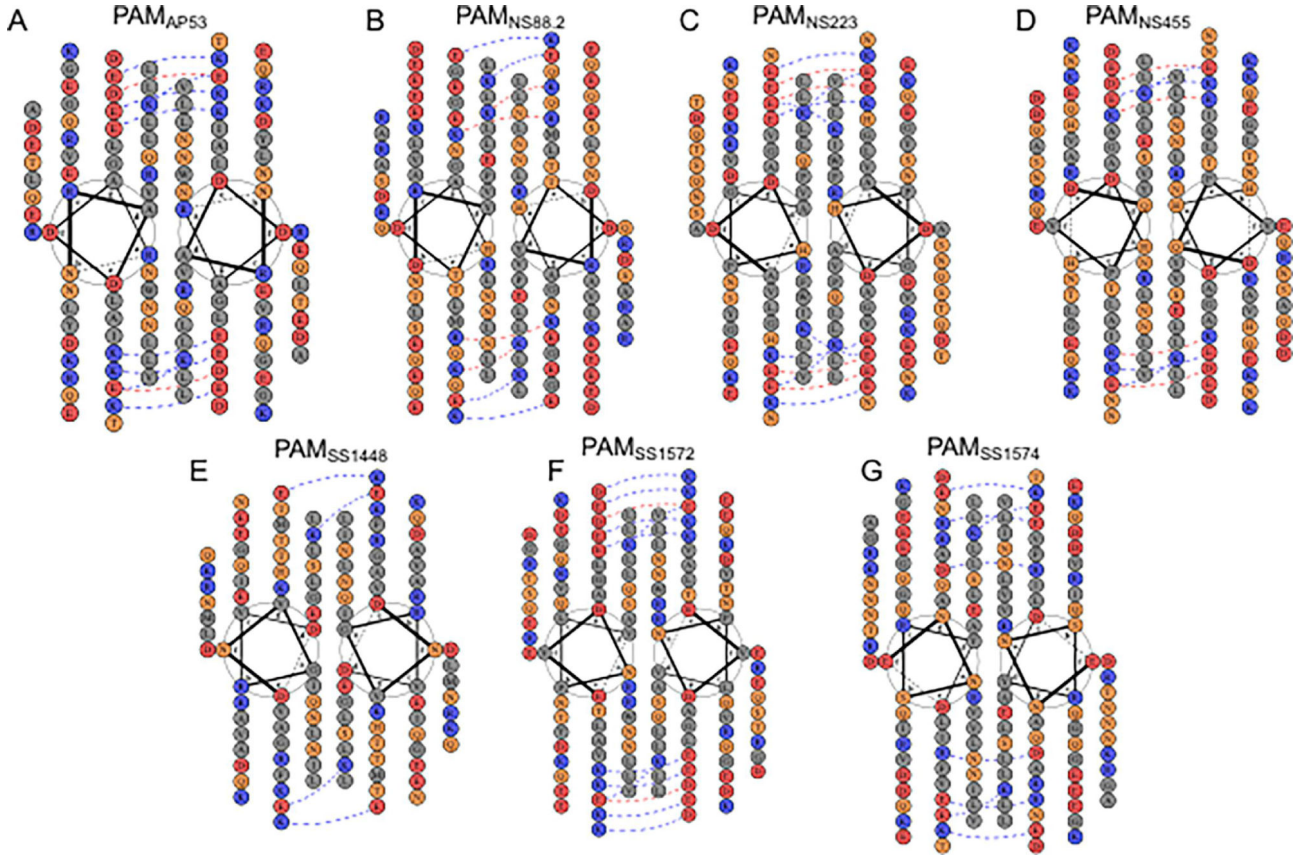

Fig. 4.

Helical wheel representations of the hypervariable region (HVR) in different r-PAMs. Construction of helical wheels for the HVR in (A) PAM$_{AP53}$, (B) PAM$_{NS88.2}$, (C) PAM$_{NS223}$, (D) PAM$_{NS455}$, (E) PAM$_{SS1448}$, (F) PAM$_{SS1572}$, and (G) PAM$_{SS1574}$ was performed using DrawCoil 1.0 (http://www.grigoryanlab.org/drawcoil/). The position of each residue is identical to that from the heptad register alignments (Fig. 3). The residues are categorized and highlighted in colored circles: grey, apolar residues; blue, positively charged residues; red, negatively charged residues; orange, polar residues. The blue and red dash lines indicate potential electrostatic attraction and repulsion, respectively, between residues at positions *e* and *g*, respectively.

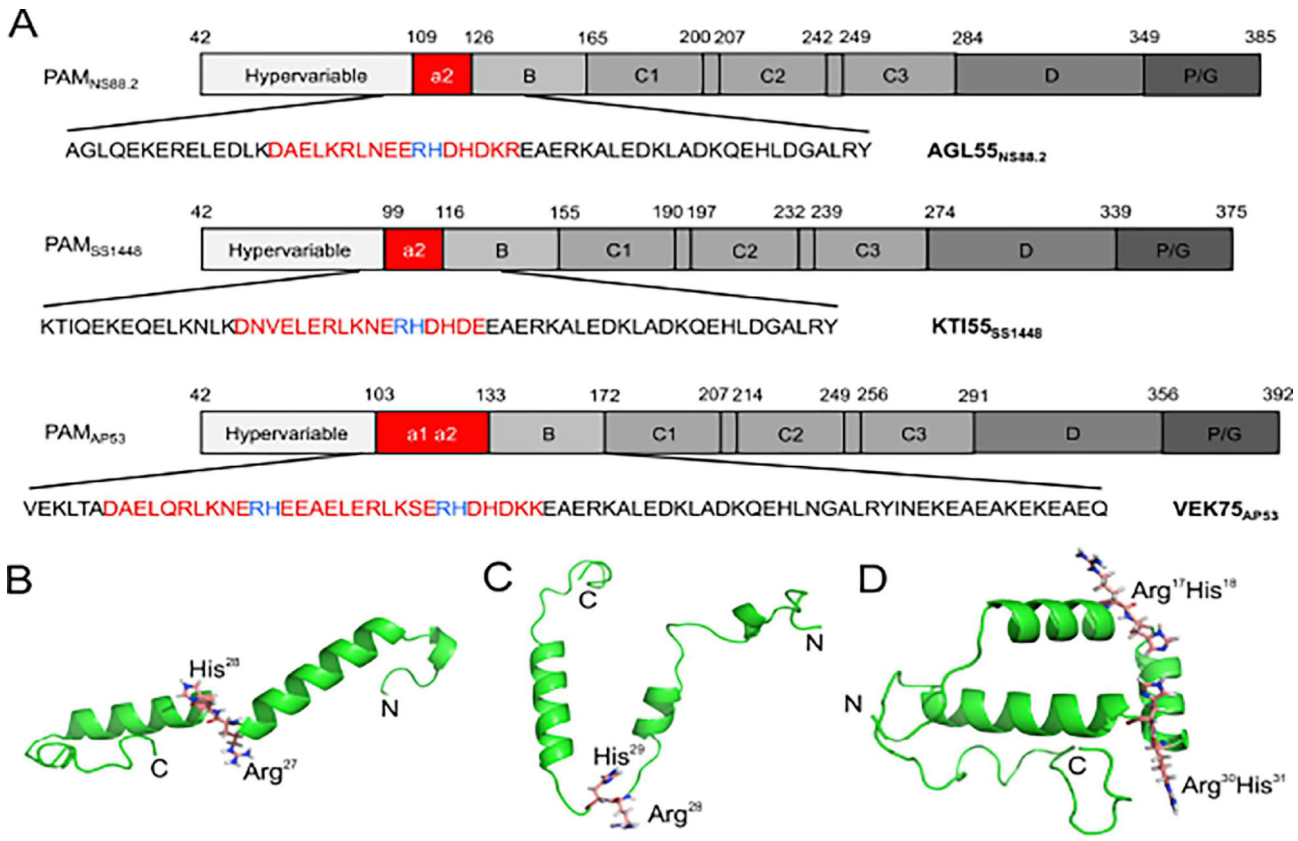

Fig. 5.

NMR solution structures of $AGL55_{NS88.2}$, $KTI55_{SS1448}$, and $VEK75_{AP53}$. (A) Coding sequences of three peptides were cloned from their corresponding naturally occurring PAMs, *viz.*, $PAM_{NS88.2}$, PAM_{SS1448}, and PAM_{AP53}. PAM-specific hPg-binding a1a2-repeats or the a2-repeat of the A-domain are shown in red. The Arg-His hPg-binding residues are shown in blue. The ribbon diagram of the lowest energy structure is presented for (B) $AGL55_{NS88.2}$, (C) $KTI55_{SS1448}$, and (D) $VEK75_{AP53}$. The Arg-His motifs are shown as sticks, and the N- and C-termini of the peptides are labeled.

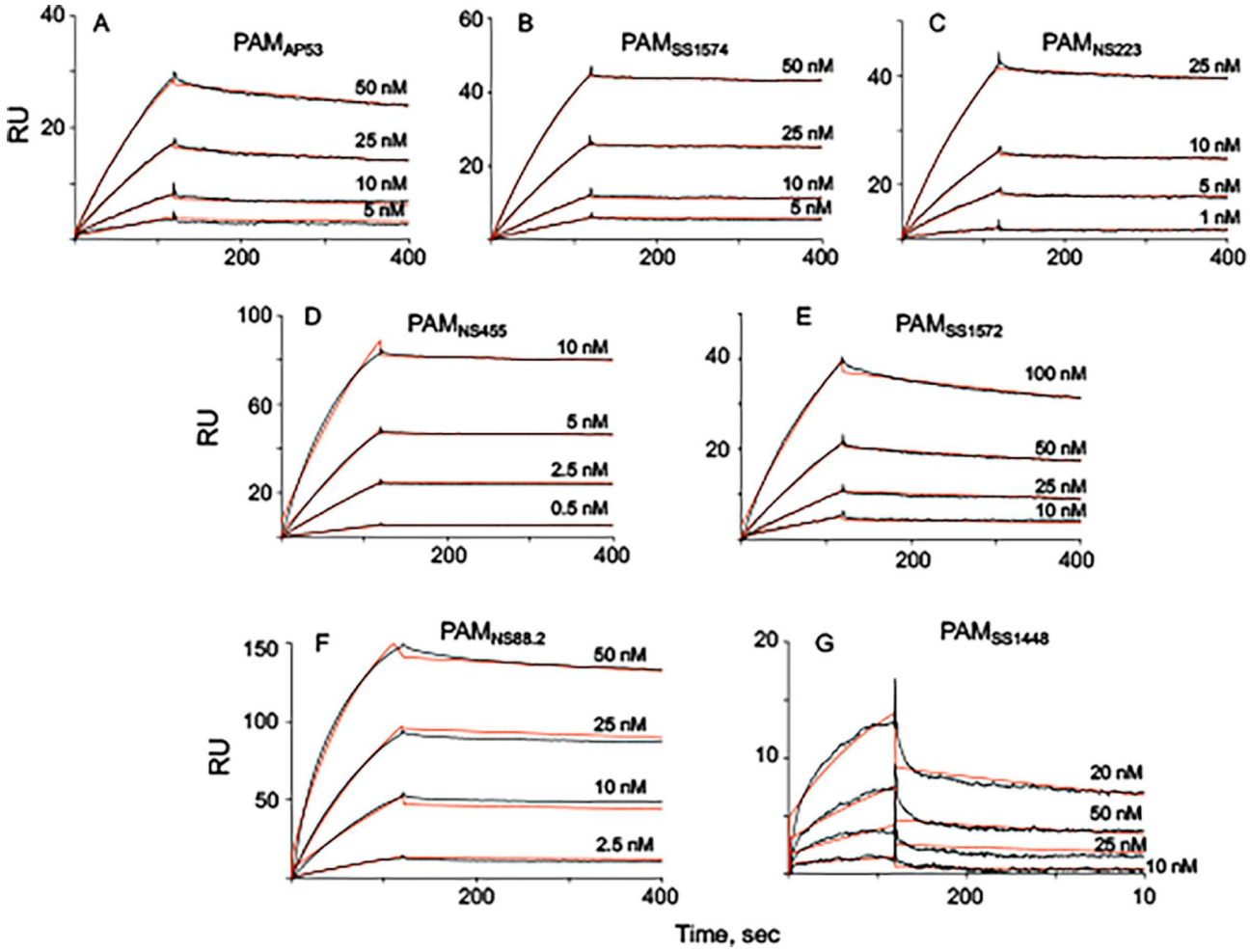

Fig. 6.

Binding assays of full-length r-PAMs to hPg. All binding experiments were conducted by SPR at 25° C. Kinetic analyses were performed for **(A)** PAM_{AP53}, **(B)** PAM_{SS1574}, **(C)** PAM_{NS223}, **(D)** PAM_{NS455}, **(E)** PAM_{ss1572}, **(F)** $PAM_{ns88.2}$, **(G)** PAM_{ss1448}. The data were fit using a 1:1 Langmuir binding model. The corresponding binding constants (K_D) for these curves were calculated from the average values of k_{off}/k_{on}, are provided in Table 3.

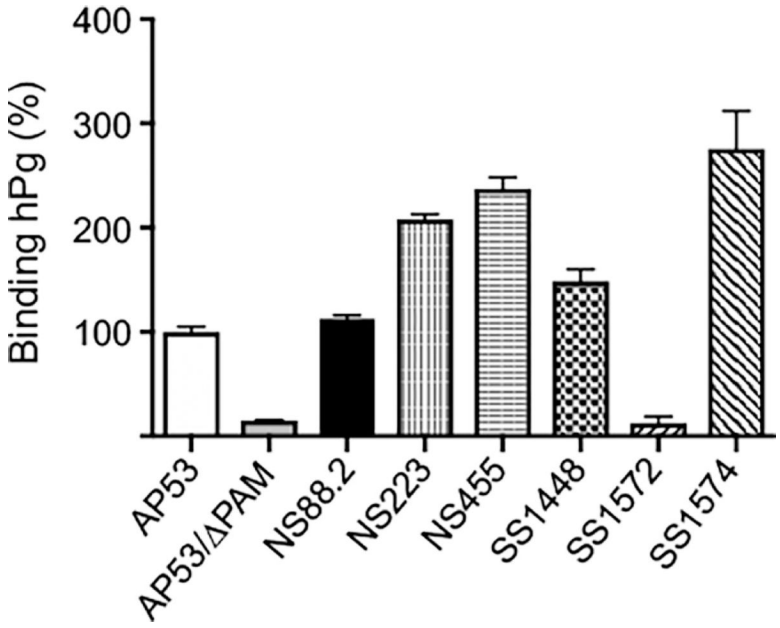

Fig. 7.

Whole cell PAM expression. After incubation of hPg with GAS, the cells were sequentially incubated with mouse anti-hPg (primary antibody) and Alexa Fluor 488-donkey anti-mouse IgG (secondary antibody). The cells were washed with PBS, pH 7.4, between incubation steps. The median fluorescence intensity at 488 nm of original histograms was used to determine the amount of cell-bound hPg. The capacity of binding to hPg for each strain was normalized to AP53, which was set at 100%. AP53/Δ*pam* was used as the negative control.

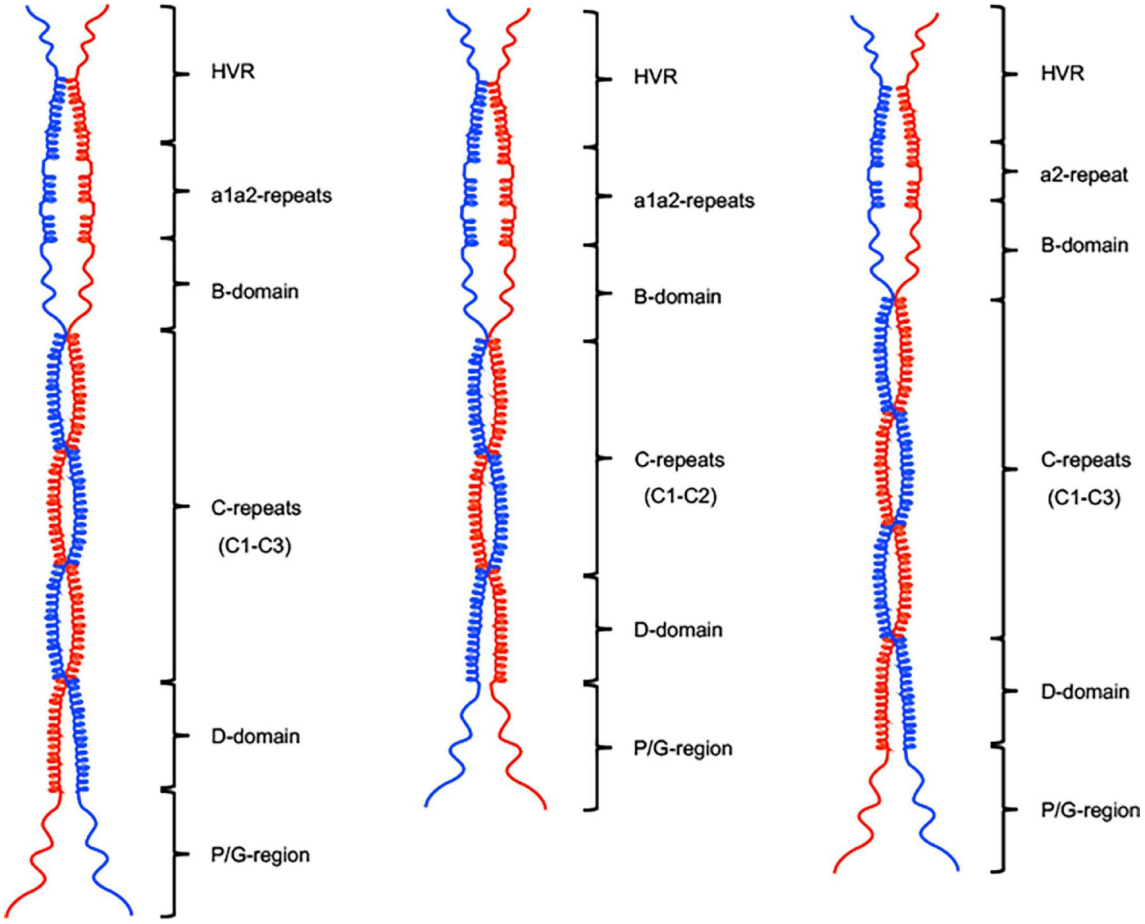

Fig. 8.

The structural model of r-PAMs. Models were drawn to scale in ChemDraw Professional 16.0. According to the results from CD, AUC, and heptad register alignments, the c-repeats of the C-domain, together with partial HVR and D-domain regions, form helical coiled-coil dimers in a rod-like conformation in solution. But a1a2-repeats and most of the B-domain manifest coiled-coil disrupting properties. (A) Class I and III PAMs, except PAM_{SS1574}, encompass three c-repeats and intact a1a2-repeats. (B) PAM_{SS1574} is the shortest among all naturally occurring PAMs due to the loss of one c-repeat, despite the complete a1a2-repeats as other Class I and III PAMs. (C) Class II PAMs, *viz.* $PAM_{NS88.2}$ and PAM_{SS1448}, lack the whole a1-repeat but express three c-repeats. In the C-domain.

Table 1.

Molecular weights and α-helical contents of naturally occurring PAMs

Protein	α-helical content[a]	Mol. Wt. calcd. (MALDI-TOF)[b]	Mol. Wt. AUC[c]	
			18,000 rpm	20,000 rpm
$PAM_{NS88.2}$	33 %	40,004 (40,020)	81,900 ± 300	81,900 ± 1,200
PAM_{NS223}	61 %	41,728 (41,760)	83,700 ± 1,000	84,800 ± 1,000
PAM_{NS455}	72 %	41,916 (42,055)	83,400 ± 1,200	80,200 ± 1,700
PAM_{SS1448}	33 %	38,544 (38,644)	77,700 ± 400	76,200 ± 900
PAM_{SS1572}	59 %	41,529 (41,635)	83,200 ± 900	84,000 ± 500
PAM_{SS1574}	54 %	37,266 (37,401)	78,800 ± 1,200	72,300 ± 300

[a] CD spectroscopy was conducted at 25° C, and the α-helix content was calculated for each protein employing the mean residue ellipticities at 222 nm.

[b] Calculated molecular mass from the protein linear sequence calculated by ExPASy and the (experimentally determined molecular masses from MALDI-TOF).

[c] Molecular weight (Mol. Wt.) of protein in solution from AUC at 25° C. In all cases, single molecular weight species was observed throughout the concentration gradient in the cell. Data from the top, top, and top channels were collected and presented as the mean ± S.D.

Table 2.

Molecular weights and α-helical contents of PAM_{Ap53} and its derivative truncated peptides

Protein	α-helical content[a]	Mol. Wt. calcd. (MALDI-TOF)[b]	Mol. Wt. AUC[c]		
PAM_{AP53_short}	39 %	16,845 (16,917)	28,000 rpm 15,200 ± 1,000	32,000 rpm 14,800 ± 2,000	36,000 rpm 14,400 ± 2,300
PAM_{AP53_medium}	32 %	20,498 (20,348)	24,000 rpm 22,700 ± 500	28,000 rpm 21,500 ± 600	32.0 rpm 18.0 ± 200
PAM_{AP53_long}	49 %	35,232 (34,937)	18,000 rpm 67,600 ± 2,500	21,000 rpm 67,600 ± 3,800	24,000 rpm 67,500 ± 4,500
PAM_{AP53}	27 %	40,941 (41,083)		81,507[d]	
$VEK75_{ap53}$		9,119 (9136)		40,000 rpm 9,700 ± 300	46,000 8,800 ± 100
$AGL55_{NS88.2}$		6,726 (6,733)		40,000 rpm 6,400 ± 200	46,000 rpm 6,700 ± 100
$KTI55_{SS1448}$		6,784 (6,791)		40,000 6,900 ±120	46,000 6,400 ± 100

[a] CD spectroscopy was conducted at 25° C, and α-helical content was calculated for each protein employing the mean residue ellipticities at 222 nm.

[b] Calculated molecular mass from the protein linear sequence calculated by ExPASy and the (experimentally determined molecular masses from MALDI-TOF).

[c] Molecular weight (Mol. Wt.) of the proteins in solution from AUC at 25° C. In all cases, single molecular weight species was observed throughout the concentration gradient in the cell. Data from the top, top, and top channels were collected and are presented as the mean ± S.D.

[d] From (Bhattacharya et al., 2014).

Table 3.

Binding kinetics of naturally occurring PAMs and truncated PAM_{AP53} to hPg at 25° C

Protein	k_{on} ($\times 10^4$ Ms^{-1})	k_{off} ($\times 10^{-4}$ s^{-1})	K_D (nM)[a]
Class 1 PAMs			
PAM_{apsb}	34 ± 15	5.6 ± 1.1	1.6 ± 0.8
PAM_{ss1574}	10 ± 3	1.1 ± 0.2	1.1 ± 0.4
Class II PAMs			
$PAM_{NS88.2}$	20 ± 4	2.3 ± 0.3	1.2 ± 0.3
PAM_{SS1448}	3.6 ± 0.7	10 ± 1	28 ± 6
Class III PAMs			
PAM_{NS223}	24 ± 9	3.3 ± 0.4	1.4 ± 0.5
PAM_{NS455}	54 ± 12	1.7 ± 0.2	0.3 ± 0.07
PAM_{SS1572}	12 ± 6	5.9 ± 0.1	4.9 ± 2.4
Truncated PAM_{AP53}			
PAM_{AP53_short}	4.0 ± 0.7	7.7 ± 1.6	1.9 ± 0.5
PAM_{AP53_medium}	2.3 ± 0.1	5.4 ± 0.9	2.3 ± 0.4
PAM_{AP53_long}	0.9 ± 0.4	1.3 ± 0.1	1.4 ± 0.6

[a] K_D values were calculated from the average values of k_{off}/k_{on} in the Table.